

OPTICAL AND ELECTRON METALLOGRAPHY OF Al SUBSTRUCTURES

by

D. W. Demianczuk

OPTICAL AND ELECTRON METALLOGRAPHY
OF ALUMINUM SUBSTRUCTURES

by

DIONISYJ W. DEMIANCZUK

A thesis submitted to the Faculty of Graduate
Studies and Research in partial fulfilment of
the requirements for the degree of Master of
Engineering.

Department of Metallurgical Engineering,
McGill University,
Montreal, Canada.

January 1967

TO MY PARENTS

ABSTRACT

The principles of the electrolytic polishing and etching of aluminum and of polarized light metallography are reviewed. Experiments are described in which aluminum was extruded to give a variety of substructures when viewed with polarized light. The same samples were also studied by scanning, replica and transmission electron microscopy and by electron diffraction. It was found that the subgrain sizes and misorientations determined optically were larger than those obtained by electron metallography, and therefore unreliable. It was also observed that the same dislocation substructure led to a wide range of optical substructures, depending on the plane of section.

A close correspondence was observed between the optical substructure and certain features of the oxide topography. However, the latter was not found to be epitaxially related to the aluminum substrate, although a loose relationship did exist. A mechanism is proposed relating the shade of the subgrains observed under polarized light to the detailed geometry of the oxide surface.

ACKNOWLEDGEMENTS

The author wishes to express his sincere thanks to Professor J. J. Jonas for his assistance, unfaltering encouragement, and constructive criticism throughout this entire work. Equally sincere thanks are due to Dr. H. J. McQueen for his contributions to this study by performing the transmission electron metallography and electron diffraction. Gratitude is also expressed to Mr. A. Rezanowich of the Pulp and Paper Research Institute of Canada for the scanning electron microscopy and to the National Research Council for supporting this work through grant number A-1634. The Aluminum Company of Canada Ltd. is gratefully acknowledged for supplying the aluminum and also the spectographic analysis of the material.

Thanks are also due to: Professors A. I. McPherson and D. R. Stevenson for their constructive discussions, the staff and graduate students, especially Mr. W. A. Wong, of the Metallurgical Engineering Department for their assistance in the theoretical and experimental parts of this work, and to Miss C. Hennessy for typing the thesis.

In closing these acknowledgements, the author also wishes to express his sincere gratitude to his parents for their continuous encouragement and support.

TABLE OF CONTENTS

ACKNOWLEDGEMENTS		i
<u>CHAPTER ONE</u>		
	INTRODUCTION	1
<u>CHAPTER TWO</u>		
	PRINCIPLES OF ELECTROLYTIC POLISHING AND ANODIC ETCHING	5
Section 2.1	Principles of Electropolishing	6
2.2	Factors Influencing Electropolishing	13
2.3	Mechanism of Oxide Formation During Anodic Etching	16
2.4	Factors Influencing Oxide Formation	22
2.5	Results of Electropolishing and Anodic Etching	23
<u>CHAPTER THREE</u>		
	PRINCIPLES OF POLARIZED LIGHT METALLOGRAPHY	26
Section 3.1	Polarization by Reflection	29
3.2	Polarization by Double Refraction	31
3.3	Polarization by Dichroic Crystals	32
3.4	Observations with Reflected Light	32
3.5	Transmission Through Transparent Dielectrics	40
3.6	Oxide Surfaces and Metallographic Observations	44
<u>CHAPTER FOUR</u>		
	EXPERIMENTAL PROCEDURE	49
Section 4.1	Material and Billet Preparation	50
4.2	Extrusion Conditions	51
4.3	Preparation of Specimens for Optical Examination	53
4.4	Preparation of Specimens for Optical Examination of Central Fiber	54
4.5	Optical Method of Measuring Misorientation Between Subgrains	55
4.6	Optical Determination of Subgrain Size	59
4.7	Effect of Varying the Oxide Coating Thickness on Contrast Between Subgrains	59
4.8	Optical Effect of Tilting Sample	60

4.9	Transmission Electron Microscopy	60
4.10	Scanning Electron Microscopy	61

CHAPTER FIVE

	RESULTS OF OPTICAL METALLOGRAPHY	63
Section 5.1	Types of Substructures Observed	64
5.2	Types of Substructures Obtained on Sectioning Selected Fibers at Different Angles	66
5.3	Misorientation Between Subgrains	69
5.4	Thickness of Oxide Coating	72
5.5	Effect of Changing the Angle of Tilt	74
5.6	Effect of Using Light of Different Wavelengths	74
5.7	Reflection from Parallel Scratches on Aluminum Surface	76
5.8	Reflection from Furrows on Overanodized Coarse-Grained Sample	77
5.9	Reflection after Applying a Metal Coating on the Oxide	77

CHAPTER SIX

	TRANSMISSION ELECTRON METALLOGRAPHY RESULTS	80
Section 6.1	Structure	81
6.2	Orientations and Misorientations	81
6.3	Replicas of Oxide Coating	84

CHAPTER SEVEN

	RESULTS OF SCANNING ELECTRON METALLOGRAPHY	87
Section 7.1	Equiaxed Substructure	88
7.2	Definitely Cross-Hatched Substructure	88
7.3	Indefinitely Cross-Hatched Substructure	91

CHAPTER EIGHT

	DISCUSSION	95
Section 8.1	Oxide Nucleation and Growth	96
8.2	Furrow Orientation and Metal Substrate Crystallography	98
8.3	Relation of Size of Regions of Uniform Furrow Orientations to Metal Substrate	100
8.4	Variation in the General Features of the Oxide Topography for Different Crystallographic Planes of Section	100

8.5	Effect of Oxide Thickness on Apparent Microstructures	104
8.6	Effect of Angle of Tilt on Contrast Between Subgrains	106
8.7	Effect of Furrow Direction on Polarization by Reflection	107
8.8	Effect of Furrow Slope on Polarization by Reflection	113

CHAPTER NINE

CONCLUSIONS	118
-------------	-----

APPENDIX	121
----------	-----

BIBLIOGRAPHY	125
--------------	-----

CHAPTER ONE

INTRODUCTION

When certain metal specimens are viewed under an optical or electron microscope, a substructure can be detected within the normal grain structure of the material. Some characteristics of this substructure are that each subgrain is usually relatively small (in the range of 1 to 100 microns) and that the boundaries between adjacent subgrains are low angle boundaries (i.e. the misorientations between the subgrains range from about a minute up to 10° or so). By comparison, the misorientations across normal grain boundaries are of the order of twenty or more degrees, and grain sizes can go up to 10^5 microns, or more.

Subgrains can, in general, be produced by a number of methods, including growth from the melt or from vapour. However, for the present purpose, only two methods will be considered: polygonization during static recovery, and polygonization during dynamic recovery. The first involves a stage of deformation followed by heating at temperatures above half the absolute melting point. In this case, on deformation, small cells outlined by dislocation tangles are formed within each deformed grain. Upon annealing, the dislocations move by glide and by cross-slip or climb, depending upon the type of dislocation, so that a considerable amount of dislocation rearrangement and annihilation occurs. Finally the cold work cells are transformed into subgrains whose interiors are relatively dislocation free, and whose boundaries are much neater and tidier than the original tangles forming the walls. The driving force for polygonization is the lowering of the elastic strain energy associated with the walls as the cells turn into subgrains, and the boundary dislocation density is decreased.

This is a recovery process since the subgrains are formed by the motion of dislocations and not by a nucleation and growth mechanism.

The second process for the formation of subgrains is polygonization during high temperature dynamic recovery. This process is peculiar to the high stacking fault energy metals. In this case, deformation occurs at elevated temperatures and polygonization, i.e. the formation of subgrains, occurs concurrently with the deformation and not subsequent to it. The driving force for this type of polygonization is still the lowering of the dislocation density, but in this case the annihilation of excess dislocations is promoted by the presence of the externally applied stress, in addition to the internal stress fields of the dislocations themselves, and to the thermal activation. Here again subgrains are formed with low angle boundaries and relatively dislocation free interiors. In general, the perfection and size of such grains depend upon the strain rate and temperature of deformation for any particular metal, and the ease of polygonization of different metals depends upon their relative stacking fault energies.

In work performed at McGill, Wong et al (1) have shown that, when aluminum is extruded at homologous temperatures of about 0.75 and strain rates of the order of 0.02 to 0.03 per sec., polygonization of the second type occurs throughout the material and no recrystallization takes place. They also showed that, for conditions of constant temperature and strain rate, the subgrain size (as determined electron microscopically) remains constant (2). However, when such specimens were investigated under the polarizing microscope by the present author, a wide spectrum of substructures was observed. These substructures,

as revealed by electrolytic etching, varied from well-defined, equiaxed subgrains, through various ill-defined directional substructures, to areas of no substructure at all.

It was not clear from the literature why such a spectrum of substructures should be observed after uniform deformation, and so the major object of this study was to determine the meaning of the various substructures, and thus allow interpretation of the optical results. As the experiments involved the polarized light examination of anodically etched samples, the following two chapters will deal with the principles of electrolytic polishing and etching, followed by the principles of polarized light metallography.

CHAPTER TWO

PRINCIPLES OF ELECTROLYTIC POLISHING
AND ANODIC ETCHING

2.1 PRINCIPLES OF ELECTROPOLISHING

The functions of an ideal electropolishing process are twofold:

- a) "smoothing" by the elimination of large-scale irregularities (above a micron in size), and
- b) "brightening" by the removal of smaller irregularities (down to about a hundredth of a micron in size).

During electropolishing, the metal to be polished forms the anode in an electrolytic cell, and continued solution of the metal occurs in such a way that the surface becomes smooth and bright. By varying the conditions of operation, the anode (specimen) can either be etched, polished, or partially or completely passivated.

If the variation of potential across the cell with anode current density is determined, a curve of the shape shown in Fig. 1 is obtained. This curve can be broken up into five main parts which are: A - B etching; B - C unstable; C - D stable plateau with polishing; D - E slow gas evolution with pitting; E - F polishing with rapid gas evolution. The optimum condition for polishing is in the area C - D adjacent to D. Thus, electropolishing can be recognized as a particular case of the more general anodic phenomenon of concentration overpotential and passivity (3, 4) which occurs in irreversible electrolytic cells.

The theories that describe the mechanism of electropolishing involve the formation of two distinct layers (5):

- i) a thin film on the surface of the anode, which controls the brightening action;

FIGURE 1

General curve relating anode current density and cell voltage in an electropolishing electrolyte.

Region A - B etching conditions

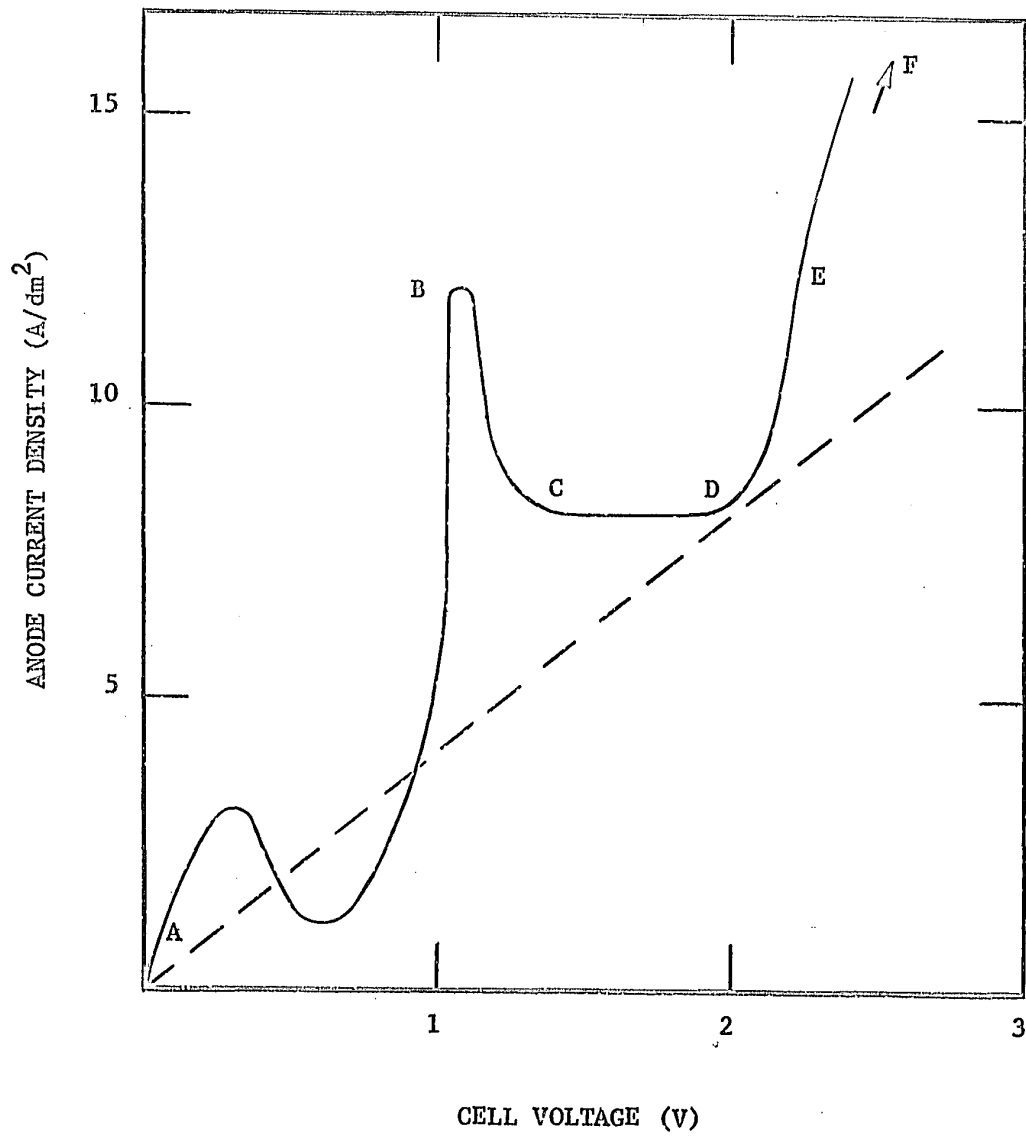
B - C unstable conditions

C - D stable polishing

D - E slow gas evolution and pitting

E - F polishing with rapid gas evolution

From Tegart (5).



- ii) a relatively thick viscous layer which controls the smoothing action. The thick layer consists of reaction products and surrounds the specimen and the thin film, as shown in Fig. 2.

Various detailed theories have been proposed for the way in which polishing occurs, though little agreement appears to exist. Some of these theories will now be outlined, although a complete review will not be attempted.

2.1.1 Smoothing

Jacquet's Resistance Theory. Jacquet (6) found the viscous layer of (ii) above to be about 50μ thick when operating in the stable polishing region. With moderate stirring, the thickness decreased to 35μ and with vigorous stirring a thickness of only about 25μ was observed (5).

He found the viscous layer to be dielectric in nature, and obtained an increasing potential at the terminals of the cell when the current density was increased. This can be seen from Fig. 1. Jacquet concluded from such results that the resistance to the passage of current was greater in the valleys, and there the current density was at a minimum. The opposite was the case for the ridges, and there the current density was at a maximum. The variation in resistance resulted in the ridges dissolving more quickly, and an effective smoothing operation taking place.

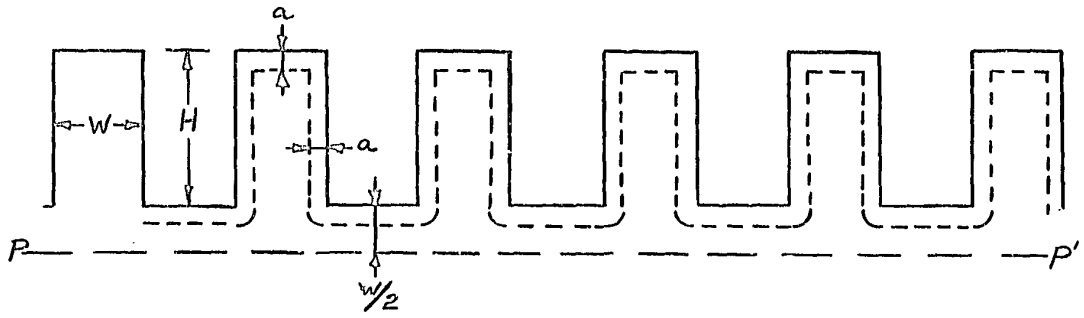
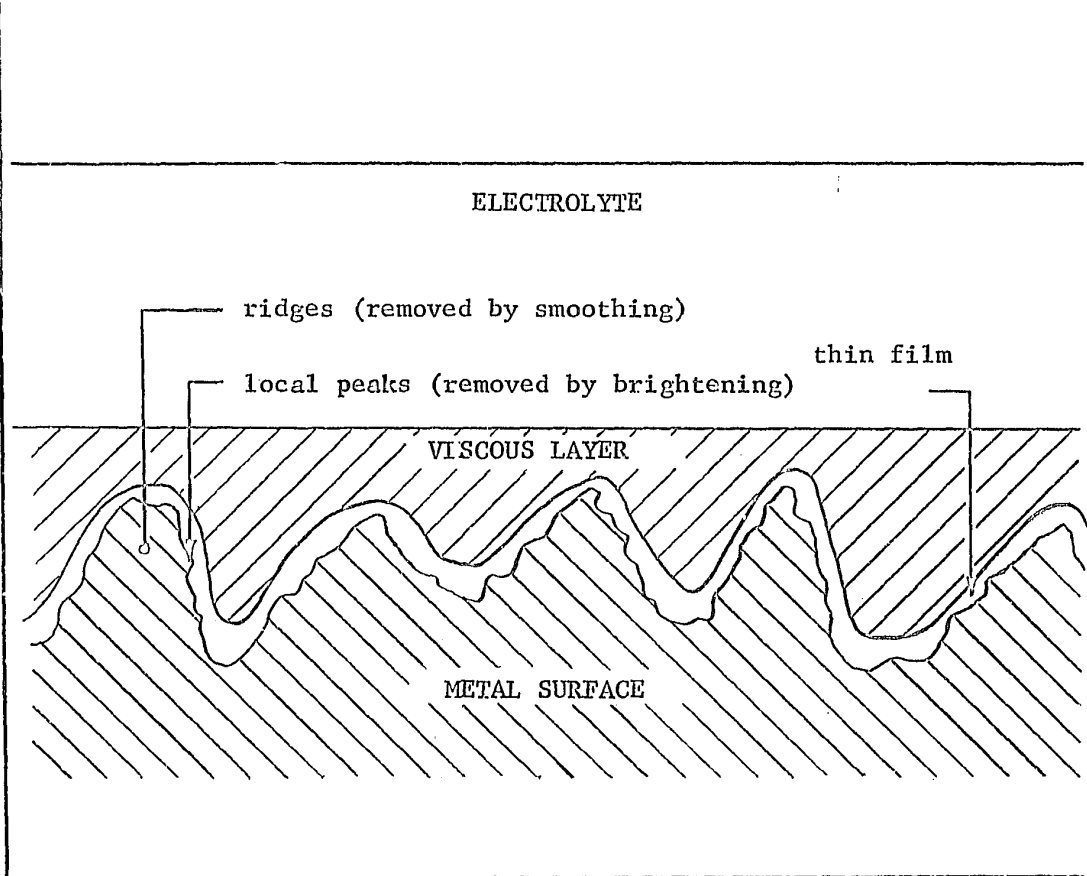
Elmore's Concentration Gradient Theory. A somewhat different explanation was proposed by Elmore (7, 8). Though he agreed that the

FIGURE 2

Schematic diagram of metal surface and viscous layers formed in electrolyte during electropolishing.

FIGURE 3

Schematic representation of dissolution of surface irregularities.



viscous film was a factor in polishing, he claimed that its insulating properties were not solely responsible for the preferred dissolution of the ridges. He proposed that the smoothing action was also due to the difference between the valley and the ridge concentration gradient in the viscous layer. Since the concentration of the solution products in the vicinity of the ridges was lower than that in the valleys, the dissolution of anodic metal from the ridges occurred at a faster rate than that from the valleys. This theory ascribes differences in layer resistance to differences in concentration gradient which in turn depend on concentration parameters.

Anion Acceptor Theory. Halfawy (9) proposed another theory of polishing suggesting that in some cases it was not so much the diffusion of metallic ions that controlled the dissolution of the metal, but rather the distribution of the anions over the ridges and depressions on the anode under the action of the electric field and the viscosity. In a related piece of work, Edwards (10) showed that the polishing effect was due to the impoverishment of the anolyte in respect of "acceptors", i.e. anions or certain polarizable molecules such as water.

2.1.2 Brightening

Most investigators believe that the brightening action of electrolytic polishes, like passivation, is connected with the formation of a very thin film on the surface of the anode. These may be the result of the partial crystallization of the products of solution, either to form complex salts or, more frequently, to form oxides (11). Other possible mechanisms are the adsorption of atoms or

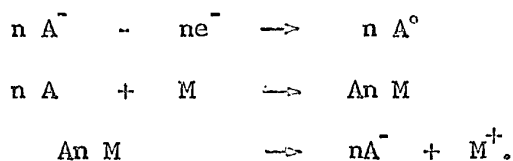
molecules of oxygen, or the adsorption of anions. The various mechanisms will now be examined in turn.

Crystallization of Complex Salts Theory. The crystallization of a complex salt (12,13), due to supersaturation of the ions during polishing, cannot easily occur at the small peaks and irregularities involved in the brightening process. It is prevented from doing so by the flow of the supersaturated film and by the diffusion of ions away from the irregularities. Conversely, salt formation is favoured at the bases of the peaks where the concentration of the salts is higher and where diffusion is more difficult. Thus brightening can be explained on the basis of the crystallization of complex salts.

Oxide Film Formation Theory. Brightening can also be analyzed in terms of potential variation and oxygen formation. The electrolyte layer in contact with the general anode surface is more quickly saturated with the dissolution products than the electrolyte near the peaks and irregularities. Thus the potential of the metal in the former areas is higher than at the peaks where diffusion is easier. The necessary potential for oxygen liberation by electrolytic means is in turn reached first in the low-lying areas. Once oxygen is liberated, but before it exists in quantities large enough to allow the formation of bubbles, a thin film of oxide is formed (14) or a layer of molecules is bound by adsorption in these areas. Both of these effects result in the electrical insulation of the low-lying areas, and in this way passivate them with respect to the peaks. This permits both brightening and polishing to take place, with the former

being observed first since the irregularities are smaller.

Adsorption of Anions Theory. Some investigators (15 - 18) consider that polishing involves the adsorption on the anode of anions of the electrolyte, especially when using electrolytes containing perchloric acid or its salts (19, 20), or fused salts for high temperature polishing. In this case, dissolution of the anode takes place by the indirect method which can be represented by the following equations:



Here, M^+ is the metal ion and A^- is the anion in solution (monovalent in this case), and may be of the form ClO_4^- . The anions are believed to set up a thin compact film about the anode, which is below the viscous layer. This film sets up an electrostatic field which is sufficiently intense to detach the metal ions from the lattice and carry them into solution. By this method both the peaks and the plains are dissolved at the same rate. However, smoothing and brightening of the surface still results, as can be seen from the following argument. Suppose that the surface irregularities are represented by equispaced, parallel, rectangular irregularities, as shown by the solid line in Fig. 3. The width of these irregularities is W , and their height is H . After a given time t , a quantity of material " a " in thickness is polished away from each surface. The new surface of the specimen is then represented by the dashed outline. Eventually " a " attains the value $W/2$ and the rectangular irregularities are replaced by smaller peaked ones. This process repeats itself until the final surface is as smooth

as desired.

The main hypotheses regarding the mechanisms of electropolishing have just been reviewed. It is the opinion of some investigators, and also of the present author, that electropolishing is a complex process, incorporating several of the above mechanisms. The principal mechanism for a particular metal/electrolyte combination then depends on the detailed conditions involved.

2.2 FACTORS INFLUENCING ELECTROPOLISHING

2.2.1 Choice of Electrolyte.

At present, electrolytes are available for polishing most metals and alloys. These are summarized in several lists (21, 22, 23) for which the following principles apply. Electrolytic polishing is most useful for polishing single phase alloys and multiphase alloys where all the phases are solid solutions. In general, it is not suitable for polishing alloys containing intermetallic phases because these have electrochemical properties that are quite different from the matrix. Different electrolytes are generally required for the polishing of different metals and in some cases, the different alloys of a given metal. There are some electrolytes that are capable of polishing several metals (5); however, such solutions are usually not acceptable for research but are useful in commercial practice for routine examination.

2.2.2 Cell Voltage and Anode Current Density.

It is possible by means of a simple apparatus to obtain values of cell potential drop, whether a potentiometric or series circuit is

used (5). A graph relating the cell potential and anode current density was shown in Fig. 1. From this graph it can be seen that varying the cell voltage will cause different reactions to take place at the anode. Along A-B the specimen is etched; at B-C instability occurs and it is possible to get periodic oscillations of the current density. At C-D, polishing occurs at constant current density. The rate of polishing as well as the quality of the polish increases as the point D is approached from C. The value of current density for this plateau is commonly called the "limiting" current density. The section D-E of the curve represents conditions at which gas evolution and pitting occur. At cell voltages much higher than E, the surface of the anode is both etched and polished. Thus, the most favourable conditions for polishing are described by the C-D part of the curve.

2.2.3 Temperature

Increasing temperature has a two-fold effect on electropolishing. With increasing temperature, the resistance of the electrolyte decreases, and thus the cell voltage required to give the same current density is less. The voltage required to obtain a given current density can generally be described by an empirical equation of the form:

$$V = K/(a\theta + b)$$

where V is the voltage, θ is the temperature and K , a , b are constants determined by the conductivity of the electrolyte, the dimensions of the cell and the current passing through the cell (24).

Also, on increasing the temperature, the viscosity of the bath decreases, making it more difficult to maintain the viscous layer on the anode, and so retarding and impairing the quality of the

polish. If the bath is too cool, it may be below the critical point for the precipitation of solid products on the anode and so again hinder electropolishing. For perchloric acid solutions, this point is about 15 - 18°C.

2.2.4 Stirring

Under normal conditions, the dissolution products tend to accumulate about the anode and stirring is necessary to allow fresh electrolyte to come into contact with the metal to be polished. Stirring is also necessary to prevent overheating of the electrolyte in the vicinity of the anode. Since the heat of reaction is usually quite large, the temperature of the electrolyte near the anode may become dangerously high; e.g. in perchloric acid - ethanol solutions, for a bath temperature of 20°C, the temperature near the anode can get as high as 60 - 70°C. At high temperatures there is a possibility of this solution burning or even exploding. It is therefore necessary that fresh electrolyte be continuously supplied. Too vigorous a stirring, however, will destroy the viscous layer and so prevent the attainment of polishing conditions. In many cases, stirring can best be accomplished by rotating or oscillating the anode rather than by agitating the solution.

2.2.5 Prior Surface Preparation

In general, the finer the initial mechanical polish, the less time is required for electropolishing though there appears to be an optimum finish in some cases (25). In aluminum, a 400 emery paper finish has been recommended. This author obtain^{ed} best results

after 0000 emery paper. If the finish is too coarse, the time required to produce a smooth surface is too long, since a large amount of the metal has to be removed. The prolonged time may also cause excessive pitting due to the build-up of temperature.

2.3 MECHANISM OF OXIDE FORMATION DURING ANODIC ETCHING

Etching is the name given to the process that makes the structure of a metal apparent under an optical microscope. This usually involves the selective solution of the polished metal surface at the grain boundaries, or else, the preferential attack of different grains, depending on their orientation, composition, or crystallographic structure. Such a process is generally referred to as chemical etching.

A different form of etching may be used in some cases to reveal the structure of a metal. In this case, the material to be etched is made the anode of an electrolytic cell and carbon, platinum, or some other suitable material is used as the cathode. Depending on the electrolyte used, one of two reactions may occur:

- a) accelerated preferential corrosion of the grain boundaries or of certain grains, as in pure chemical etching; or
- b) the formation of an oxide film on the anode which produced a visible structure under the microscope. (Sometimes special microscopic techniques must be used to show up the structure, such as polarized

light or phase contrast.)

As oxide film formation played an important part in this investigation, it will be considered in more detail below.

2.3.1 Detailed Mechanism of Oxide Formation

Most metals, with gold as a notable exception, are unstable at room temperature when in contact with oxygen under atmospheric conditions and have a thermodynamic tendency to form oxides (26). In the case of aluminum, after electropolishing, an oxide coat several tens of Ångströms thick is present, as has been stated earlier. If the metal in this condition is made the anode of an electrolytic cell, where the electrolyte does not dissolve the oxide at an appreciable rate, the applied voltage will set up an electrostatic field in the oxide. This field, in turn, produces growth of the oxide film by causing metal or oxygen ions to move through the film. Oxide growth is, then, a phenomenon of ionic conduction at high field strengths, which involves two interfaces: metal/oxide and oxide/solution. Ionic transfer must occur at both these interfaces.

2.3.2 Porous and Non-Porous Oxides

The exact mechanism of oxide growth on aluminum in a hydrofluoric acid - ethanol - water electrolyte (which was used in the experiments described below), has not been investigated per se. However, it can be classified under the general study of the formation of porous oxides on the valve metal group* (26). It is generally

* The valve metal group includes such metals as Ta, Nb, Al, Zr, Hf, W, Bi, and Sb.

accepted (27) that the anodic aluminum oxide formed in an acid bath consists of two layers: a non-porous, barrier layer adjacent to the metal and a much thicker porous layer above the barrier layer.

In the initial stages of anodizing, a continuous, compact oxide film is formed, possessing a nearly constant thickness. If, at a particular point, the film is momentarily thinner than elsewhere, current is concentrated at that point and the thickness is built up. However, as the limiting thickness (14.5 \AA/volt) is approached, the growth of this film becomes slow, and the limiting thickness is approached asymptotically, until the non-porous layer finally ceases to grow.

The oxide film thickness can increase to a considerably greater extent, though, by the growth of the porous oxide, whose thickness is governed only by the length of time the voltage difference is maintained across the metal/electrolyte boundary. The porous film generally begins to grow before completion of the growth of the non-porous barrier layer, and continues to grow simultaneously with it. If the porous film is present, the barrier layer is believed not to reach its final limiting thickness since the resistance to flow of the anions or cations through both films becomes equal to the driving force at a lower value of the barrier layer thickness.

2.3.3 Ion Mobility

In order to determine the exact mechanism of oxide formation, it is first necessary to determine whether the anion, cation, or both are the mobile ions. In the case of aluminum, in a number of different electrolytes, it was suggested by Plumb (28), Amsel (29), and Rummel (30)

that the migrating substance was the metal ion.

In 1962, Davies et al (31) maintained, on the other hand, that oxygen was the ion undergoing transport. In 1963, Davies et al presented two papers suggesting that both metal and oxygen ions were mobile and migrated to form the oxide (32, 33). In 1965, using radioactive Xe^{125} , Davies et al (34) confirmed that aluminum oxide was formed by both aluminum and oxygen ion migration. They also showed that the amount of aluminum dissolved in the ammonium citrate electrolyte which they used could be very high.

From these results it can be seen that the method of transport and solubility of the metal in the electrolyte vary considerably, depending on the electrolyte chosen, the anode current density, and the voltage of the system under consideration. For barrier layer formation, it can be assumed that oxygen is the mobile ion. For the formation of the porous layer, the work of Plumb (28) most closely resembles the experimental conditions used by the present author, so that metal ion migration may be the operative mechanism.

2.3.4 Oxide Cell Formation

The mechanism of formation of a porous layer which is somewhat soluble in the electrolyte was investigated by both Evans and Keller and associates. Evans (27) maintained that Al^{+++} is the mobile ion, and assumed that the limiting thickness of the barrier layer is never reached. Thus, cation movement continues through the oxide and "most of the E.M.F. falls over the barrier layer". Of the aluminum ions, part enters the liquid producing a salt solution, keeping the

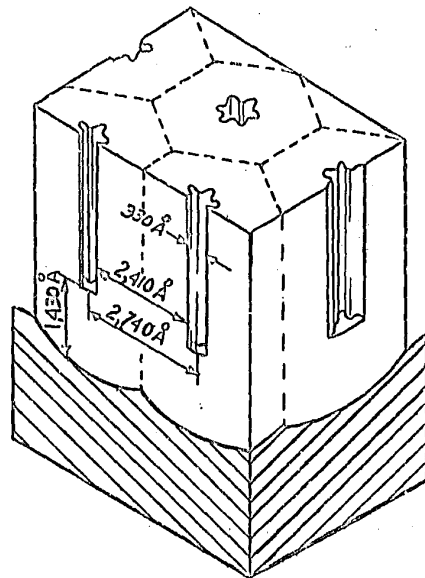
film porous, while the other part forms fresh oxide at the solid part of the porous film, pushing outward the solid matter already present. This allows the film to thicken indefinitely.

Keller et al (35), on the other hand, first considered the formation of a single cell of oxide "by virtue of the solvent action at a single point", i.e. where a locally high rate of dissolution already exists. This causes a higher current to flow at that particular point, and there follows an associated increase in temperature which further increases the rate of dissolution. This mechanism is believed to result in the formation of a pore which is illustrated in Fig. 4. The above picture can only hold if the effect of the temperature rise is greater than the effect of the increased current; i.e. that the increase in solubility of the oxide is greater than the increase in the rate at which oxide is formed due to the increased current, each taken from an equilibrium value.

Assuming that a stable pore is formed, and that current flows through it, oxide is continuously being created and dissolved. If the pore acts as a point source of current, the current field and the voltage field are spherical, and the advancing front of the oxide cell also tends to be spherical. Since the cell walls cannot be thicker than the limiting value (14.5 \AA/volt for the potential drop between the pore face above the barrier layer and the electrolyte outside the wall), a cylindrical cell is formed, having a roughly hemispherical end and a central cylindrical pore. Because the oxide cells must completely cover the anode surface, they cannot be perfectly cylindrical, however, and adopt a hexagonal structure. A similar mechanism

FIGURE 4

Schematic representation of a porous oxide cell
formed on anodic etching. From Keller (35).



produces a star-shaped configuration in the central pore. The structure of a cell which agrees with these considerations was shown in Fig. 4.

2.3.5 Cell Formation and Subgrains

It is interesting to note here that Keller observed that single rows of cells form along either side of a subgrain boundary in aluminum. This is said to occur because at these points the amorphous oxide film is discontinuous, and therefore offers less resistance to the flow of current. Once nucleated, the cell structure fills in the subgrain area, and if further growth is allowed, the identity of some of the subgrains may even become masked.

2.4 FACTORS INFLUENCING OXIDE FORMATION

Of the factors that influence the type of oxide coating obtained, the electrolyte seems to be predominant. In borate, tart-rate, succinate, citrate, phosphate or carbonate solutions, the oxide is non-porous and has high ionic resistance. This type of film is generally amorphous. It grows in a very short time to a certain limiting thickness, depending only on the applied voltage. The films formed in sulphuric, phosphoric, oxalic, or hydrofluoric acid solutions, on the other hand, are generally porous (above the barrier layer) and have a low ionic resistance. They usually have lower dielectric strengths for a given ionic current than the other films.

The operative distinction between the two classes of electrolyte is probably that porous films are formed in an electrolyte which dissolves the oxide at an appreciable rate, while no dissolution takes

place during the formation of the non-porous films. Other cell variables, in general, only have an effect on the kinetics of film formation, which are excellently reviewed by Young (26), and will not be touched on in this treatise.

2.5 RESULTS OF ELECTROPOLISHING AND ANODIC ETCHING

It has been stated that for aluminum polished in a perchloric acid-ethyl alcohol electrolyte, an oxide film thickness of several tens of Ångströms is observed immediately after polishing (19, 36). It is possible that this oxide film results from operation for a short period of time in the etching stage of the curve shown in Fig. 1. Another possibility is that it results from the adsorption of oxygen ions on the surface of the metal during the polishing operation. In either case, this film, and the oxide layer formed during anodic etching, may be expected to possess somewhat similar properties.

In 1949, a furrow-like structure was first reported on an electropolished surface by Brown (37) and by Bucknell (38). In 1957, Welsh (39) investigated this phenomenon more closely and found that the "furrowed" pattern was not the only one obtainable. He also obtained a "dotted" and a "globular" pattern. Each of these could be obtained using a perchloric acid-alcohol electrolyte, but under different conditions of applied potential and bath temperature. The conditions can be summarized as follows:

- 0 - 10 v. (applied potential) - no detectable structure
- 10 - 20 v. - furrow structure

20 - 30 v. - transition from furrow to dotted structure
30 v. and up to breakdown limit - dotted or globular
structure, the latter appearing only at
temperatures below 0°C and potentials
exceeding 40 v.

In 1952, Bucknell et al (40) and Bussy (41) plotted their results stereographically and showed the range over which the furrow orientations were straight and parallel. Their results may be summarized as follows: on faces near (100) orientations, the lines were, with minor deviations, constant in the $\langle 100 \rangle$ direction. As the orientation changed towards the (100) or the (111) poles, less regular patterns were observed. On or near (111) faces, the furrows changed into rows of granules.

Thus it may be seen that under certain conditions of electro-polishing in perchloric acid-ethanol electrolytes, an oxide layer is formed on the surface of the metal. This oxide layer has a definite structure which seems to bear some relationship to the metal substrate.

Several investigators have determined that the surface after anodic etching in a 2% hydrofluoric acid, 49% ethanol, 49% water electrolyte is also striated. The striations or grooves are parallel or nearly so (42 - 47). The groove spacing can vary from part of a micron to several microns, depending on the thickness of the oxide coating. After short anodizing times (1 - 2 minutes), no striations were detected by polarized light inspection; however, using phase-contrast, small striations were observed (47). Increasing the anodizing time to about 15 minutes led to striations of several microns spacing,

which are visible under polarized light (42). It was also shown by Hone (42) that the grooves of highly over-anodized surfaces penetrate to about one quarter of the oxide thickness. These striations or grooves do not form in perfectly parallel rows, but are of the same overall direction, although in the short range they may differ by 5° to 10° from the general direction. The ends of such grooves may be oriented by as much as 45° to the overall direction of the furrows. An example of such an over-anodized film is seen in Fig. 6 of the paper by Pearson et al (44).

Returning now to the overall process of anodic etching, it is known that the microstructure of aluminum can be revealed by the use of polarized light metallography in conjunction with electrolytic etching. When a given sample is rotated with respect to the plane of incident polarized light, regions of the sample change from black to white through shades of grey, or through different colours if a sensitive tint plate is used. For a specific orientation of the specimen, particular shades of grey or particular colours will consistently be observed. It remains now to examine the principles of polarized light metallography, in order that the manner in which the oxide coating produces this effect may be determined.

CHAPTER THREE

PRINCIPLES OF POLARIZED LIGHT METALLOGRAPHY

This chapter consists of a brief description of plane polarized light and certain of its characteristics. It is not intended as a review of the physics of polarized light since this is well covered in a number of texts on the topic (49 - 53). It is presented, rather, to emphasize some of the characteristics which enable the microscopic technique used in the optical investigation to be effective.

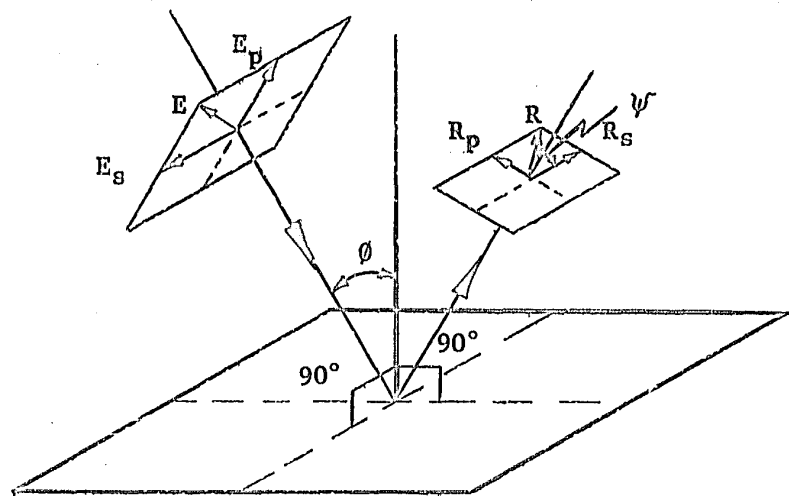
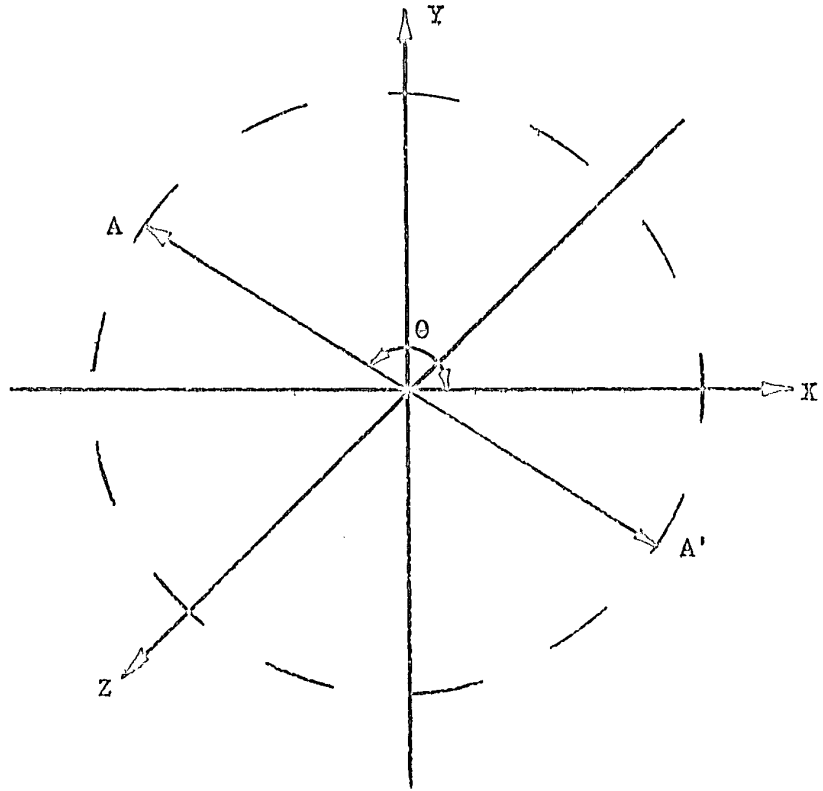
Light can be described as a transverse electromagnetic wave where the oscillating quantities are the electric and magnetic vectors which are perpendicular to each other. It has been shown by Weigner's experiment (54) that the electric vector produces the observed effects and can therefore be identified as the "light vector". If we assume, as in Fig. 5, that a beam of light is travelling in the Z^+ direction, the light vector may, at a given instant, be pictured as executing a vibration, the amplitude and direction of which are indicated by AA'. The light beam then may be described as a linear vibration of varying amplitude with sudden random changes in orientation (θ) occurring at time intervals of the order of 10^{-8} sec. If the vibrations are restricted to being linear, though of varying amplitude, and the angle θ (defined in Fig. 5) is not permitted to change, the light is said to be plane polarized, and is in a plane containing the Z axis and is oriented at an angle θ to the X axis. The azimuth angle (ψ) of plane polarized light (illustrated in Fig. 6) is defined as the angle between the plane of vibration of the incident light and the plane of incidence, the latter being the plane containing the incident beam and the normal to the surface of incidence at that point. The

FIGURE 5

Representation of vibrations of light by vector AA' , where AA' changes in amplitude and orientation θ .

FIGURE 6

Azimuths and amplitudes of plane polarized light reflected externally from a dielectric surface.



azimuth angle of the reflected light is similarly defined with respect to the plane of reflection.

Plane polarized light may be produced by several means which include the following three processes: reflection, double refraction and passage through a dichroic sheet. These will now be examined in turn.

3.1 POLARIZATION BY REFLECTION

It was found that when ordinary light is reflected from a dielectric like glass, the reflected light is plane polarized when the angle of incidence assumes a certain critical value called Brewster's angle. Brewster's law states that when the refracted and reflected rays are 90° apart, the reflected ray is plane polarized and the angle of incidence at which this condition is met depends only on the refractive index of the dielectric. The refractive index (n) is defined as

$$n = \frac{\sin \theta}{\sin \theta'} \quad (1)$$

where θ and θ' are the angles of incidence and of refraction respectively. If $\bar{\theta}$ is the angle of incidence at which the reflected ray is plane polarized (see Fig. 7), then by Brewster's law, the angle ROT is 90° and $\sin \bar{\theta}' = \cos \bar{\theta}$. Therefore

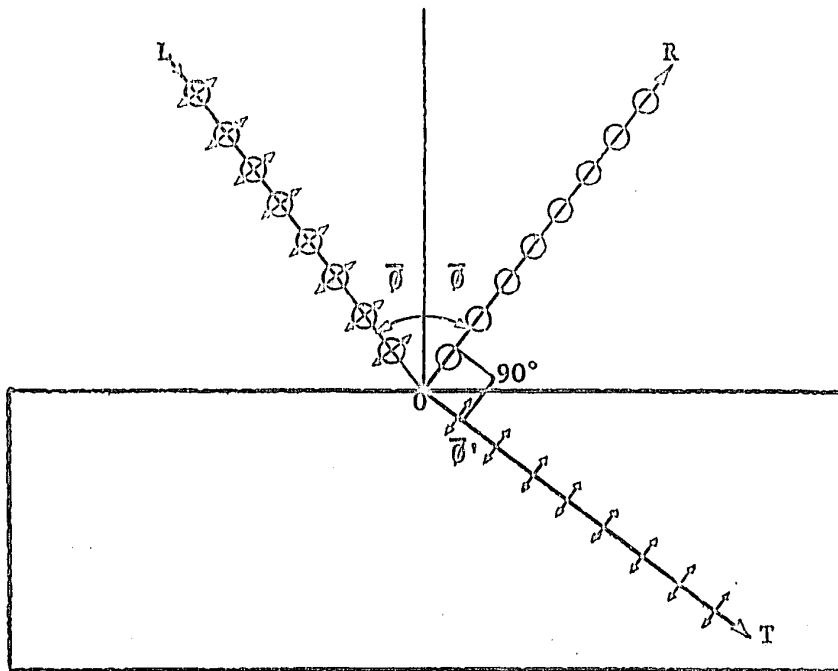
$$n = \frac{\sin \bar{\theta}}{\sin \bar{\theta}'} = \frac{\sin \bar{\theta}}{\cos \bar{\theta}} = \tan \bar{\theta} \quad (2)$$

So that Brewster's angle is $\tan^{-1} n$.

This principle also applies to the production of polarized light by reflection from a pile of plates. If the angle of incidence

FIGURE 7

Reflection from and transmission through a transparent dielectric material, when the angle of incidence is equal to Brewster's angle.



is not exactly Brewster's angle, the reflected ray is only partially plane polarized.

3.2 POLARIZATION BY DOUBLE REFRACTION

Double refraction is observed to a lesser or greater degree in all transparent crystals that are anisotropic, i.e. ones in which the physical properties vary with direction. All crystals, except those belonging to the cubic system, are anisotropic and in these, the axis of highest crystallographic symmetry is called the optic axis. The anisotropic crystals, e.g. calcite, mica, quartz, etc. demonstrate the phenomenon of double refraction or "birefringence" when light enters the crystal along a direction other than the optic axis. When the light travels along the optic axis, the phenomenon of birefringence is not observed.

For light travelling other than along the optic axis, the incident ray of light is divided into two beams, termed the ordinary (O) and extraordinary (E) rays. The O ray always lies in the plane of incidence while this is not general for the E ray. The O and the E ray travel at different speeds through the crystal. The relative retardation, d , divided by the thickness of the crystal is called the birefringence. Also the planes of polarization of the O and E rays are perpendicular to each other, i.e. the amplitudes of vibration are oriented at 90° to each other.

The production of plane polarized light by double refraction is best illustrated by the nicol prism, which removes one of the two

refracted rays by total reflection. The constructional details of a common nicol prism can be seen in reference (49).

3.3 POLARIZATION BY DICHOIC CRYSTALS

These crystals have the property of selectively absorbing one of the two rectangular components of ordinary light; generally it is the O vibrations. The result is that only vibrations perpendicular to the O vibrations are transmitted and so plane polarized light is obtained. The most common dichroic crystal is tourmaline and it produces plane polarized light when the optic axis of the crystal is parallel to the face of the tourmaline plate.

It is also possible to have polarizing films with properties similar to those of tourmaline but which have been artificially prepared. Such films are called "Polaroid" films. They contain sulphate of iodoquinine, which forms a mass of ultramicroscopic needlelike crystals that are made to align themselves in one direction. Each tiny crystal behaves optically like a thin plate of tourmaline. When ordinary light passes through such a film, it emerges as plane polarized light. At the present time, Polaroid sheets are commonly used as polarizers and analysers in optical apparatus.

3.4 OBSERVATIONS WITH REFLECTED LIGHT

If the possible conditions that may arise on inspection of a metal covered with a transparent oxide are considered, it will be noticed that:

- 1) the oxide layer may be isotropic or anisotropic.
- 2) the metal may also be isotropic or anisotropic.
- 3) the oxide may be doubly refractive or optically active and have various possible orientations of its optic axis with respect to the incident light.

With regard to the metallography of aluminum, the processes that must be considered are the following: reflection at the air/oxide interface; reflection at the oxide/metal interface; and transmission through the transparent dielectric. These items will be considered in turn in the following sections.

3.4.1 Reflection from an Isotropic Dielectric

In this case, the amplitude vector of the incident beam of plane polarized light (E) can be resolved into two components, one perpendicular (E_s) and one parallel (E_p) to the plane of incidence, as in Fig. 6. The azimuth angle (ψ_R) of the reflected ray (R) can be calculated from the following equation:

$$\tan \psi_R = \frac{R_p}{R_s} = \frac{E_p \cos (\theta + \theta')}{E_s \cos (\theta - \theta')} \quad (3)$$

Here the subscripts p and s represent the parallel and perpendicular components, respectively, of the incident and reflected rays, and θ and θ' have been defined previously.

Equation (3) is based on Fresnel's law of reflection which may be expressed as follows:

$$\frac{R_s}{E_s} = -\frac{\sin (\theta - \theta')}{\sin (\theta + \theta')} \quad (4a)$$

$$\frac{R_p}{E_p} = \frac{\tan(\theta - \theta')}{\tan(\theta + \theta')} \quad (4b)$$

From these two equations, several interesting quantities can be found. For any angle of incidence, the reflectance (r) of a particular material can be calculated from equation 4 since

$$r_s = \frac{(R_s)^2}{(E_s)^2} \quad (5a)$$

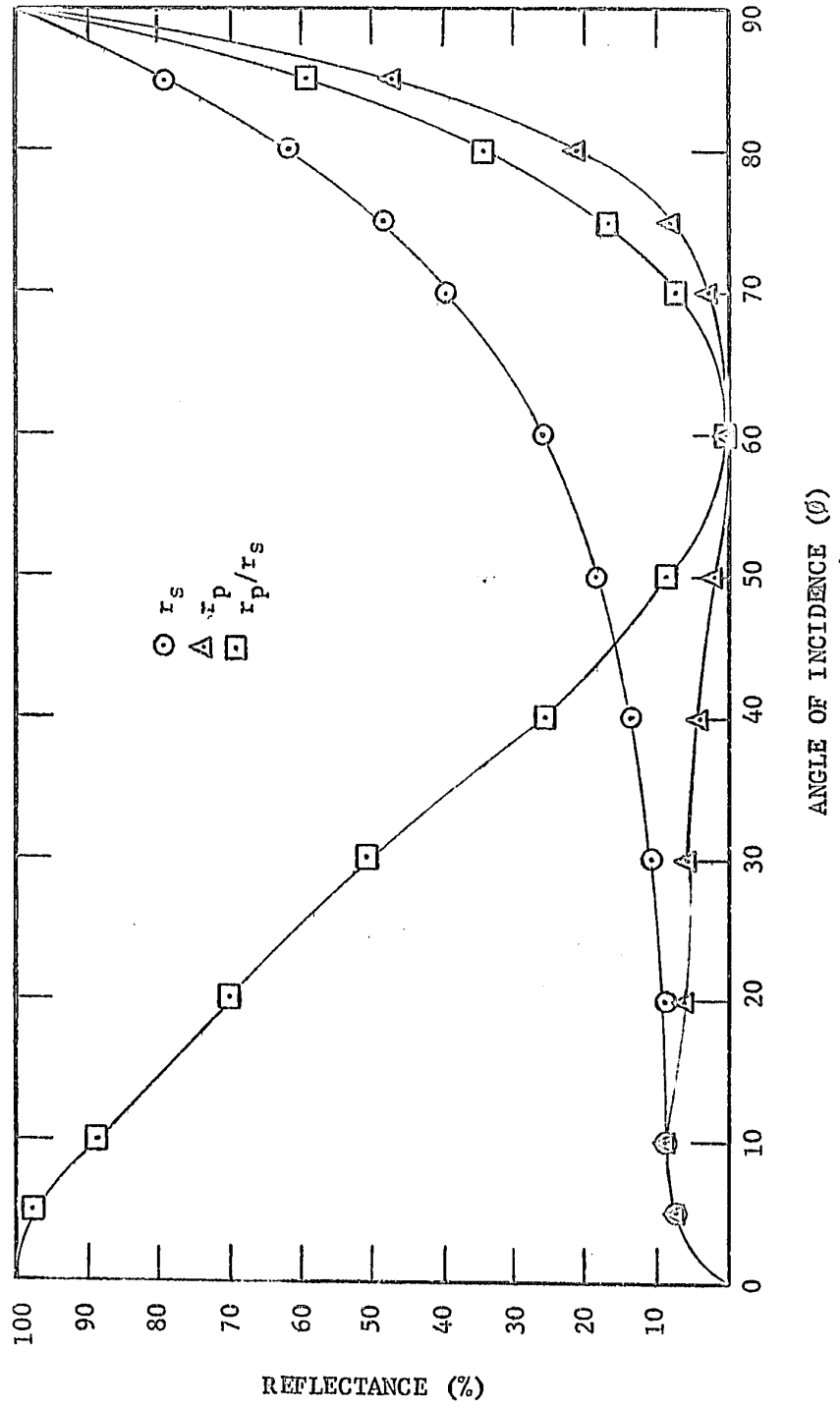
$$r_p = \frac{(R_p)^2}{(E_p)^2} \quad (5b)$$

A plot of these reflectances is shown in Fig. 8 for $\alpha\text{-Al}_2\text{O}_3$. It is interesting to note that for small angles of incidence, only a small portion of the light is reflected, and that for high angles of incidence, the amount of light reflected is relatively large. Use will be made of this fact in a later section. It should also be noticed that, at specific values of θ , the p and s reflectances are usually different. Thus there is a change in the relative amplitudes of the p and s vibrations after reflection, so that the plane of polarization of the reflected beam is rotated away from that of the incident beam. The amount of rotation depends both on the angle of incidence and on the orientation of the plane of polarization with respect to the plane of incidence, as can be seen from equations (3) and (4).

From equation (4a) it can also be seen that the sign of $\frac{R_s}{E_s}$ is always negative. This means that reflection produces a phase difference of 180° between the incident and the reflected light. For the p or parallel component, the sign is positive for small θ , indicating no phase change. When $(\theta + \theta')$ reaches 90° , the denominator

FIGURE 8

Reflectances for $\alpha - \text{Al}_2\text{O}_3$, of the components perpendicular and parallel to the plane of incidence of polarized light.



in equation (4b) goes to infinity and then there is a 180° phase change. A plot of the phase difference between the p and s components of the reflected light is shown in Fig. 9.

3.4.2 Reflection from an Anisotropic Dielectric

The effect of anisotropy in a dielectric material upon the reflection of polarized light has not been thoroughly investigated to date. However, it can be assumed that, as in the case of isotropic dielectrics, the reflectivity is highest at high angles of incidence and the absorptivity is highest at low angles of incidence. It is also probable that the optical properties depend on crystallographic orientation, although the form of the dependence is not known in detail. With regard to reflection from such dielectrics, the effect of anisotropy would be most significant at high angles of incidence where the reflectance is highest, and least important at normal incidence.

3.4.3 Reflection from an Isotropic Metal

If plane polarized light strikes the surface of a metal, it will, in general, be reflected as elliptically polarized light (49, 50). This is so since, on reflection from a metal, a phase difference is introduced between the p and s components.

The effect of introducing a phase difference between the p and s components can be seen from the addition of two sine waves of the same frequency, but having displacements in two perpendicular directions. If we choose the Y Z plane, and therefore the Y and Z directions, the two components may be expressed as

$$Y = a_1 \sin (\omega t - \epsilon \mathcal{L}_1) \quad (6)$$

FIGURE 9

The phase difference between p and s components ($\tilde{\mathcal{D}}_p - \tilde{\mathcal{D}}_s$) for a dielectric and for three metals of increasing absorption index (49).

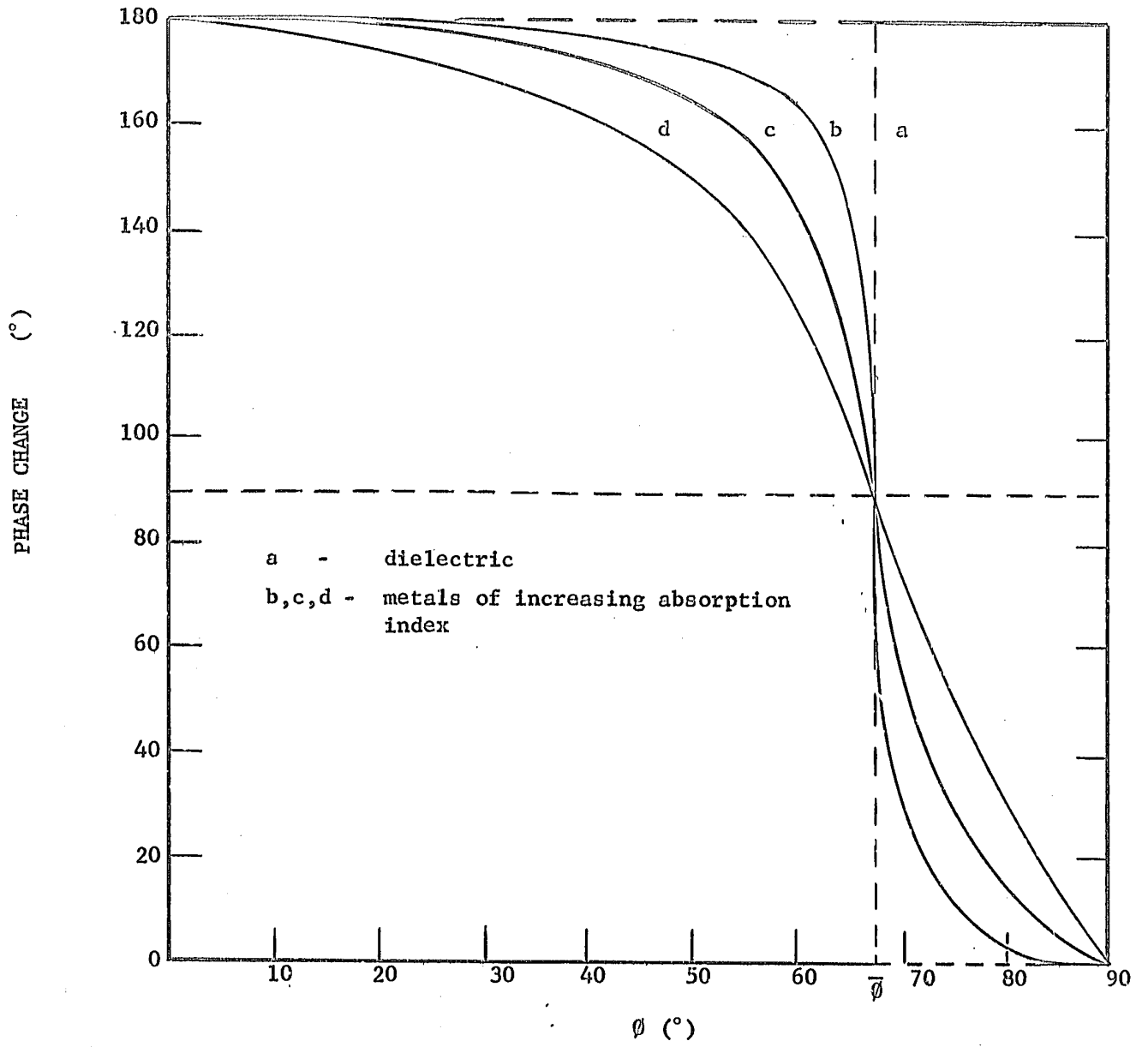
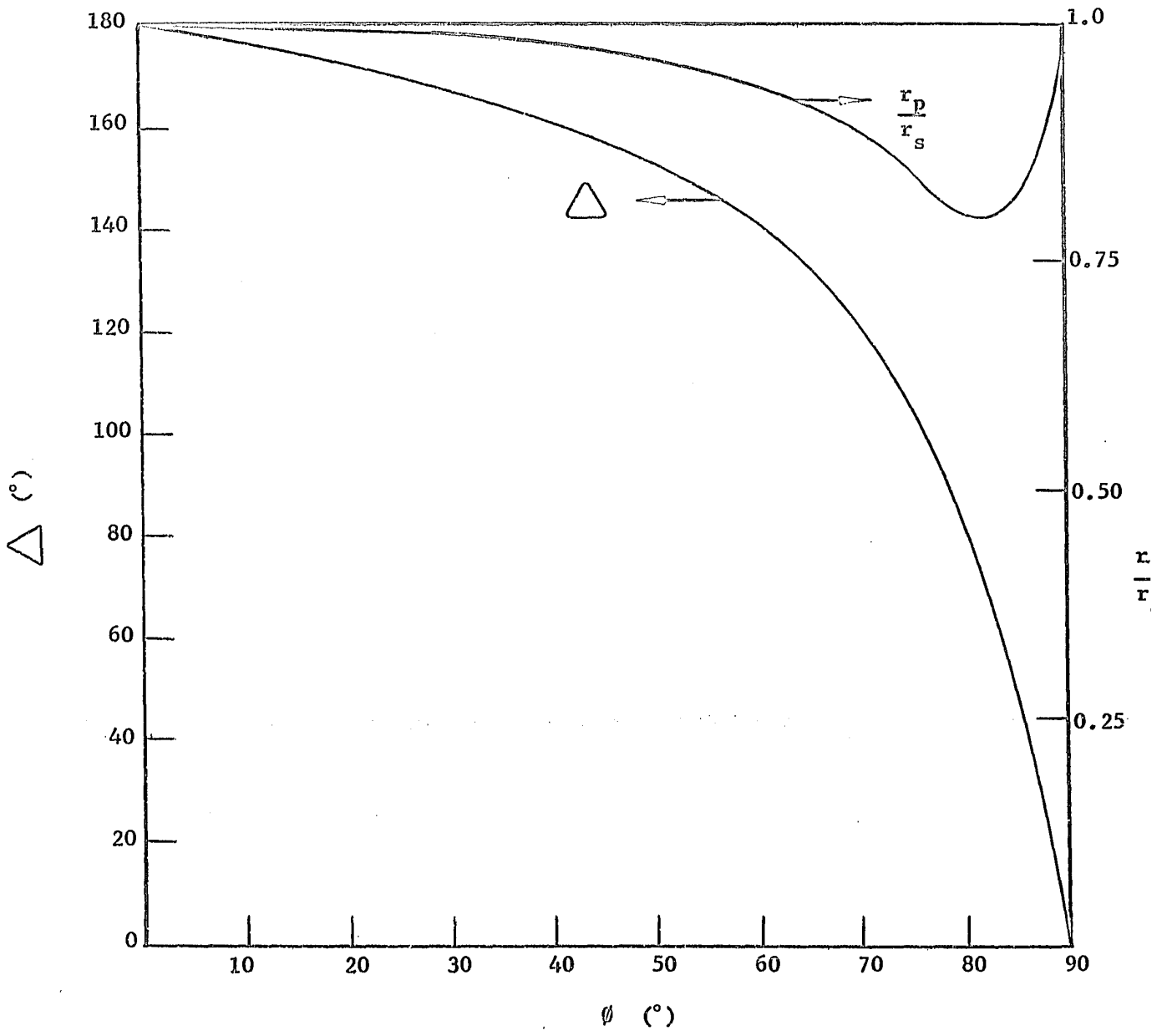


FIGURE 10

Relative amplitude quotient (r_p/r_s) and relative phase difference (Δ) for the p and s components on reflection from aluminum (27).



$$Z = a_2 \sin (\omega t - \alpha_2) \quad (7)$$

Here Y and Z are the instantaneous vibration amplitudes along the respective axes, a_1 and a_2 are the maximum amplitudes of vibration, ω is the angular frequency of vibration, and α_1 and α_2 are the respective phases at time t equals zero.

Now, on squaring each equation and subtracting to cancel the t terms, the following is obtained as the equation of the resultant path.

$$\sin^2 (\alpha_1 - \alpha_2) = \frac{y^2}{a_1^2} + \frac{z^2}{a_2^2} - \frac{2yz}{a_1 a_2} \cos (\alpha_1 - \alpha_2) \quad (8)$$

This is the equation of an ellipse and the phase difference (Δ) = $(\alpha_1 - \alpha_2)$. Thus it can be seen that a plane polarized beam is converted to elliptically polarized light on reflection from a metal surface.

If the incident light is not plane polarized, as above, but elliptically polarized, the light reflected from the metal is still elliptically polarized, with the phase difference and the amplitude between p and s components in the reflected light being different from that of the incident light. It must be remembered that plane and circularly polarized light are only extremes of elliptical polarization.

3.4.4 Reflection from an Anisotropic Metal

Anisotropy means having different physical properties in different crystallographic directions. Some of the properties that vary with direction are the reflectivity and phase difference between the p and s components. As a consequence, for any particular com-

combination of angle of incidence and orientation of the plane of polarization, different orientations of the metal lead to different amounts of rotation of the plane of polarization. For example, if a polished polycrystalline specimen of an anisotropic metal such as zinc is inspected under polarized light, the different grains are seen in different shades of grey, depending on the amount that the plane of polarization of the reflected ray is rotated into the plane of the analyser. The amount of rotation of the plane of polarization depends on the crystallographic orientation of the grain with respect to the plane of polarization of the incident light. This effect was investigated by Jamin (55) in 1847, with succeeding work by Dayton (56) in 1935. This topic is also excellently reviewed by Mott and Haines (57).

3.5 TRANSMISSION THROUGH TRANSPARENT DIELECTRICS

The behaviour of the portion of the light that is refracted into the transparent anisotropic surface layer must now be considered. Under typical conditions of small angles of incidence, this can constitute about 90% of the total incident radiation, as can be seen from Fig. 8, above. In the study of the transmission of light through an anisotropic substance, three different cases must be considered:

- a) the optic axis is parallel to the direction of normal incidence.
- b) the optic axis is perpendicular to the direction of normal incidence.
- c) the optic axis is at an angle to the direction of

transmission of light.

These cases will now be examined in turn.

3.5.1 Optic Axis Parallel to the Direction of Normal Incidence

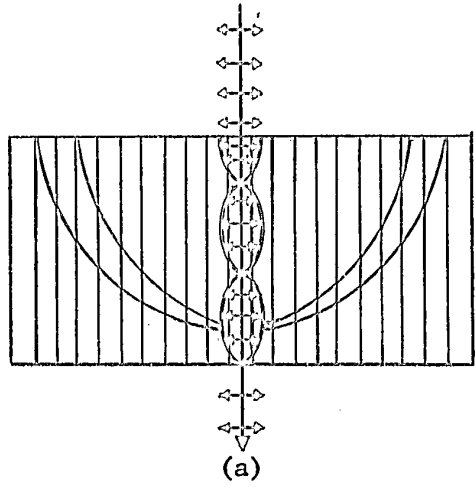
To simplify this discussion it is possible to make use of a principle of mechanics which states that any simple harmonic motion in a straight line may be considered as the resultant of two opposite circular motions. Then, according to Fresnel, plane polarized light entering a crystal along the optic axis can be decomposed into two circularly polarized vibrations, R and L, each rotating in opposite directions with the same frequency.

If the anisotropic substance is not optically active, the R and L motions travel at the same speed through the layer and their resultant at any point along the path is simple harmonic motion in the plane of original vibration.

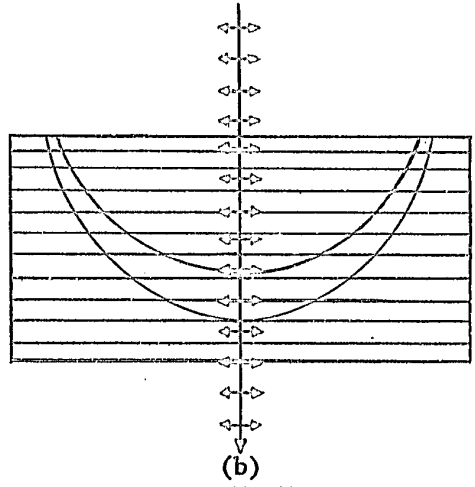
If the substance is optically active, the two circular vibrations move forward with very slightly different velocities. The result of this is that the plane of polarization rotates as the beam passes through the material (Fig. 11a). If polarized monochromatic light is used, only rotation of the plane of polarization is observed; if polarized white light is passed through the optically active material, rotary dispersion is obtained. This is due to the fact that different colours (light components of different wavelengths), are rotated by different amounts. It has been found that the amount of rotation is very nearly proportional to the inverse square of the wavelength (49). If such light is viewed through an analyser, it will be seen that the

FIGURE 11

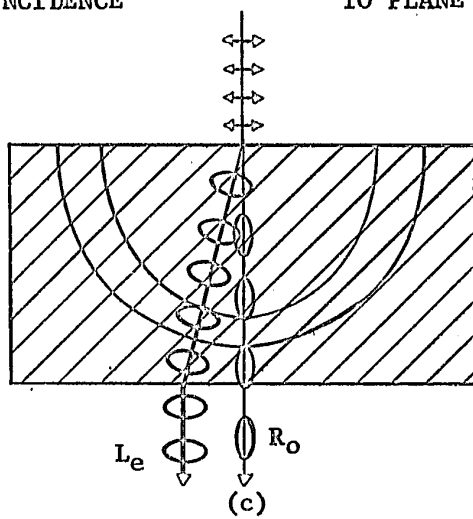
Transmission through an optically active crystal at different angles to the optic axis.



(a)
OPTIC AXIS PARALLEL
TO PLANE OF INCIDENCE



(b)
OPTIC AXIS PERPENDICULAR
TO PLANE OF INCIDENCE



(c)
OPTIC AXIS AT ANGLE
TO PLANE OF INCIDENCE

light is coloured, since light of certain wavelengths is eliminated to a greater extent than that of others.

The total amount of rotation of the plane of polarization is dependent on the total thickness of the optically active material. Usually this material is a single crystal, e.g. a single crystal of quartz but it can also be a liquid. The property of optical activity is not general for all anisotropic materials but is limited to specific cases such as quartz, cane sugar solutions, etc.

3.5.2 Optic Axis Perpendicular to Light of Normal Incidence

When the optic axis of the oxide is parallel to the surface of the metal, an incident beam perpendicular to it is not affected by the anisotropic material, whether it is optically active or not. This means that plane polarized light continues as plane polarized light in the original plane of polarization (Fig. 11b).

3.5.3 Optic Axis at an Angle to Normally Incident Light

When the optic axis is not perpendicular to the incident light, the effects of optical activity are seen to a greater or lesser extent, becoming greatest when the axis is parallel to the direction of incidence. When the incident vibrations lie in the principal section (i.e. the plane containing the optic axis and the normal to any cleavage face), they are decomposed, on entering the crystal into two ellipses L_E and R_O of different size (Fig. 11c). The major axes of these ellipses are at right angles to each other and their senses of rotation are opposite. Except when the angle between the incident ray and the optic axis is very small, the intensity of the ray R_O is

very low and L_E is a very slim ellipse. The result of this is that two rays are emergent from the optically active material and the one of greater intensity (L_E) is elliptically polarized. The major axis of this ray lies in the same plane as the plane of vibration of the incident light.

When the beam of light reaches the oxide/metal interface, it is reflected by the bright metal. On reflection, this light travels back through the dielectric, following the same interactions with the material as it did on entering this medium. This has already been discussed. It is then refracted again on entering air, a rarer medium, from the dielectric.

3.6 OXIDE SURFACES AND METALLOGRAPHIC OBSERVATIONS

In Chapter Two, it was stated that after electropolishing of aluminum, in some cases, a thin oxide film is found on the surface of the specimen. After electrolytic etching by means of anodizing, an oxide film of considerably greater thickness is present on the metal surface. In both instances, various topographic features can be detected on the outer surface of the aluminum oxide. The metallographic examination of these surfaces, both after electrolytic polishing and etching, revealed microstructures which would not have been apparent on inspecting the untreated metal surface. Several theories have been presented to explain the effectiveness of the etching technique in revealing the structure of the metal substrate. These will now be considered in turn.

3.6.1 Optical Anisotropy Theories

In 1947, Huber and Gangler (48) put forward the proposition that the grains of aluminum appeared in different shades when observed through crossed polarizers as a result of the optical anisotropy of the aluminum oxide coating. They maintained that oxide "crystals", which were anisotropic, grew in a manner which had a definite relationship to the metal matrix. These authors suggested that the oxide crystals were optically uniaxial in some cases, while in others they were optically biaxial. The uniaxial crystals were so oriented that the optic axis was normal to the surface of the metal, so that no apparent rotation of the plane of polarization of the incident light resulted. The biaxial crystals, on the other hand, resulted in different amounts of rotation of the plane of polarization of the incident light, depending only on the angle between the incident plane of polarization and the bisectrix of the biaxial crystal. They displayed a stereographic plot on which they indicated the planes where they considered the uniaxial and biaxial crystals to be formed, and they also indicated the directions of the bisectrix of the biaxial crystals in the appropriate regions.

Barker (61) in 1950 and Woodard et al (62) in 1951, working with different electrolytes, supported the opinion that the apparent structure is visible under polarized light as a result of the anisotropy of the oxide surface.

3.6.2 Topography Theories

Several investigators determined that, under certain condit-

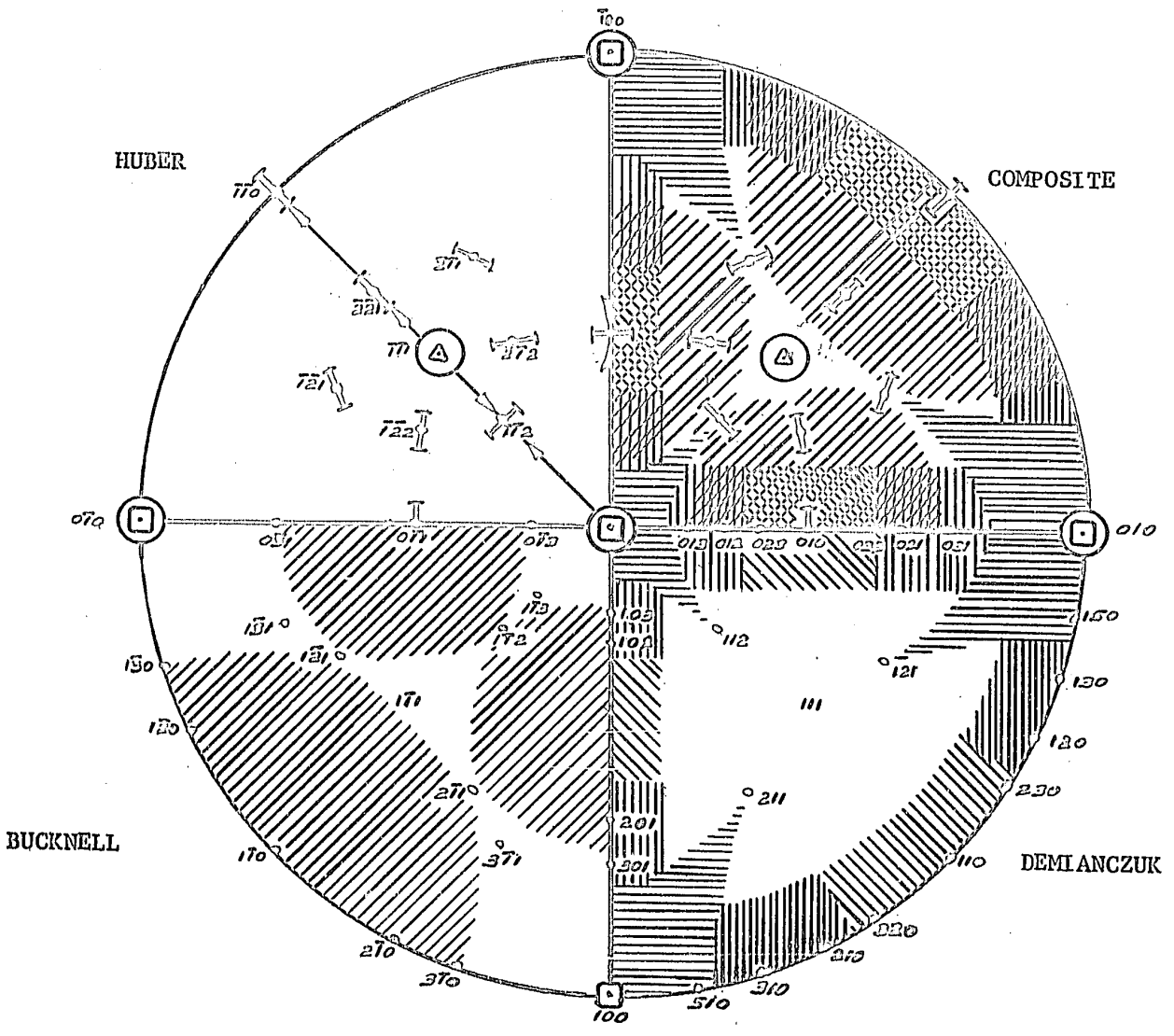
ions of polishing and etching, the surface of the oxide film can have a striated appearance due to the presence of parallel grooves or furrows (39, 42, 43, 55). On large grained samples, the striations or grooves were found to change direction from grain to grain and were believed to be related to the aluminum substrate (39). Welsh (58) suggested that the striae in aluminum were parallel to traces of the $\langle 100 \rangle$ directions on the surface. It has also been suggested (39) that the striae observed after electropolishing and those observed after anodizing bore identical relationships to the crystallography of the substrate. Bucknell et al (40) observed that a furrowed structure was present on the polished and etched face only when that face was associated with particular planes of the crystallographic lattice. The planes on which a furrowed structure was observed were plotted on a stereogram and are presented in Fig. 12.

The authors referred to above discuss the presence of a furrow structure on the surface of the oxide, but do not come to any conclusions regarding its optical effects. In 1951, Perryman (63) showed that the effect of polarized light is dependent on the topography of the surface and that it depends on the orientation of the furrows with respect to the plane of polarization of incident light. He based his arguments on his own experimental results and on the supporting evidence of Baeyertz (64), who used both a scratched surface and lamellae of pearlite to show the effect of an irregular surface on polarized light. These results are in agreement with a theory for the reflection of polarized light from irregular surfaces put forward by Jones (66).

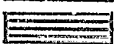
FIGURE 12

Standard 100 stereographic projection incorporating the following results:

- (a) Bucknell et al. (40), showing the surfaces on which a furrow structure was observed in recrystallized material;
- (b) Huber et al. (48), showing the projection of the bisectrix of what was considered to be an optically active biaxial crystal; or the location where no optical activity was observed;
- (c) Present author, indicating regions where the different substructures were observed.
- (d) The composite quadrant shows that there is agreement between the three sets of results.



LEGEND:

-  projection of plane of bisectrix
-  optic axis normal to surface
-  region of furrows
-  equiaxed substructure
-  definite cross-hatch
-  indefinite cross-hatch

no visible substructure about the (111) planes of section.

3.6.3 Other Theories

A similar furrow structure was observed by Wilsdorf et al (59) on specimens of aluminum containing alloyed copper. These authors agreed that the structure was not due to plastic deformation, as first suggested by Brown (37), but implied that the furrows were due to the preliminary stages of precipitation of copper. Nevertheless, they reserved the possibility that the furrowed topography may be the result of electrolytic polishing or etching.

Berghezan (60) was the first to note the appearance, under the optical microscope, of a substructure by the use of this etching technique and very short etching times (in the range of 15 to 30 secs.). In his work, some subgrains were visible in the one micron size range, while in other cases, subgrains were visible when the average size was 10 to 15 microns. No mention was made of a furrow structure but he suggested that the variation in colours observed between subgrains could be attributed to an interference effect involving polarized light. (No mention was made of the use of a sensitive tint plate.)

These are, in summary, the major proposals for the effectiveness of the polarized light technique in observing grain structures in aluminum.

CHAPTER FOUR

EXPERIMENTAL PROCEDURE

4.1 MATERIAL AND BILLET PREPARATION

The material used in the investigation was 1S aluminum supplied by the Aluminum Company of Canada Ltd, in the form of 1.5 inch diameter rods, 12 feet in length. These rods had been extruded by Alcan under the following conditions:

ingot size	9" dia. x 25" long
die reduction	36 : 1
ingot reheat temperature	445°C
press container temperature	440°C
ingot extrusion temperature	440°C
extrusion speed	120 f.p.m.
extrusion cooled by circulated air.	

The composition of the material, as determined by spectrographic analysis*, was:

Cu	Fe	Mg	Mn	Si	Zn	Ga	V	B
0.008	0.26	0.008	0.008	0.09	0.006	0.014	0.007	0.001
Ni	Ti	Bi	Cr	Pb	Sn			

all less than 0.005%.

The billets were prepared by cutting the as-received material into 4 inch lengths, facing the ends on a lathe to obtain flat parallel surfaces, and strain-annealing each billet to obtain a grain size of 10 to 15 mm. Strain-annealing was necessary to ensure uniformity of structure and to produce a large grain size in the billet so that each

* Courtesy of R. Langdon, Aluminum Company of Canada Ltd., Montreal.

grain could be followed through the die into the extrusion. This is discussed more fully in Appendix I.

The conditions finally selected for strain annealing were: preanneal at 640°C for three hours; strain in compression 3.8 - 4.0%; final anneal at 640 ± 5°C for 48 hours.

4.2 EXTRUSION CONDITIONS

After preparation as above, the billets were extruded by the direct method on a 150 ton vertical hydraulic extrusion press following the procedure outlined by Wong (65). The dies used were square-shouldered, with circular apertures 0.247 inches and 0.494 inches in diameter, resulting in extrusion ratios of 40:1 and 10:1 respectively. This led to reductions in area of 97.5 and 90.0%.

Extrusion was performed over the homologous temperature range of 0.74 to 0.79, and ram speeds from 0.022 to 0.032 inches per second were used. The latter resulted in strain rates in the range 0.7 to 0.8 per second for the 40:1 die, and 0.11 to 0.16 per second for the 10:1 die. The detailed conditions of extrusion are presented in Table I.

TABLE ICONDITIONS OF EXTRUSION

Test No.	Temperature		Ram Speed inches/sec.	Extrusion Ratio
	T_h	°C		
1	0.740	417	0.0222	40 : 1
2	0.745	422	0.0250	40 : 1
3	0.745	422	0.0310	10 : 1
4	0.745	422	0.0323	10 : 1
5	0.750	427	0.0232	10 : 1
6	0.750	427	0.0305	10 : 1
7	0.755	431	0.0235	40 : 1
8	0.760	436	0.0265	40 : 1
9	0.760	436	0.0264	10 : 1
10	0.775	450	0.0265	40 : 1
11	0.780	455	0.0242	40 : 1
12	0.790	464	0.0222	40 : 1

4.3 PREPARATION OF SPECIMENS FOR OPTICAL EXAMINATION

1. 1.5 inch lengths were cut from the 0.247 inch rods and 1/8 inch lengths from the 0.494 inch diameter rods.
2. Longitudinal sections were then prepared by using a special clamp to hold the sample, and reducing it to nearly a half-section on a rotating belt grinder, using varsol as a lubricant.
3. This was followed by hand polishing on 0, 00, 000 and 0000 emery papers, again using varsol as a lubricant. Washing between the different papers was done with acetone.
4. The samples were electropolished for 2 to 3 minutes following the method described by Raether (19). A solution of 16.7% commercially concentrated (70%) perchloric acid in ethanol was used in conjunction with a carbon cathode. Optimum polishing conditions were obtained at a cell voltage of 18 - 20 volts, a current density of 3 - 4.6 amp./in.² (48 - 73.6 amp./dm.²), and a temperature of 20 ± 2°C.
5. The specimens were electrolytically etched for 2 to 3 minutes in a solution containing by volume (47):

49 parts	ethanol
49 parts	distilled water
2 parts	hydrofluoric acid (48%).

A cell voltage of 40 to 60 volts was used, with a current density of 0.40 to 0.60 amp./in.² (6.4 to 9.6 amp./dm.²), and a super-purity aluminum cathode. The bath temperature was also $20 \pm 2^\circ\text{C}$.

4.4 PREPARATION OF SPECIMENS FOR OPTICAL EXAMINATION OF CENTRAL FIBER

The variation in the apparent substructure with the angle of section was investigated as follows. Using the 10 : 1 die, extrusions were made with the aim of producing one with a single grain or fiber running axially down the center of the extrusion. Each extrusion was examined for such a fiber by taking 1/8 inch samples every six inches along the length of the extrusion.

The first and second steps were identical to those mentioned above, except that great care was taken to remove just less than half of the sample on the belt grinder. Steps three and four were then repeated successively until the section was within fifty microns of the exact center of the original specimen. The sample was then etched as described in step five.

Inside - outside calipers were used to mark the center of the extrusion on the polished surface. These markings were made by fine scratches. The sample was then inspected under a Vickers projection microscope with a high pressure xenon light source. All the optical observations were carried out with crossed polarizer and analyser, using white light.

If the sample did not contain a relatively large fiber

running centrally down the extrusion axis, it was discarded, and the next sample taken six inches away along the extrusion was similarly tried. If the specimen did contain such a fiber, it was investigated as follows.

Similar 1/8 inch samples were cut from the adjacent material on either side of the original sample. Each sample was polished, by the method described above, at different angles to a reference line (S_1) previously inscribed on the surface of the extrusion. The angle of section was determined by measuring, on the surface of the rod, a distance equal to the arc subtended at the surface by the required angle. This distance was marked on the rod surface by a fine scratch (S_2) (see Fig. 13a).

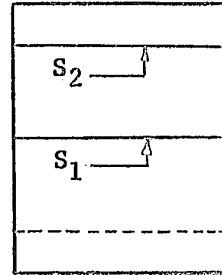
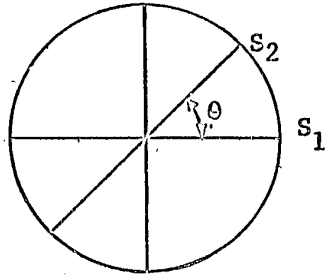
The specimen was then placed in the polishing clamp (Fig. 13b), after ensuring that the surface of the rod was in contact with the semi-circular portion of the clamp and that the scratch (S_2) was aligned with the lip of the clamp (see Fig. 13c). Care was taken to ensure that each specimen was positioned in the same way and the technique was estimated as being accurate to $\pm 3^\circ$ of the quoted value.

4.5 OPTICAL METHOD OF MEASURING MISORIENTATION BETWEEN SUBGRAINS

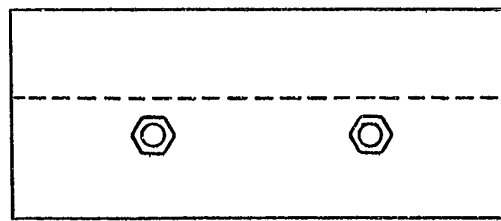
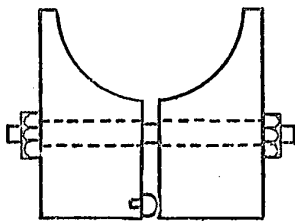
The sample was mounted on the Vickers projection microscope so that the extrusion axis was horizontal on the screen when the stage protractor read zero degrees. If a substructure was visible, the type of substructure was noted. The stage was then rotated in one direction until this structure appeared in maximum contrast, that is,

FIGURE 13

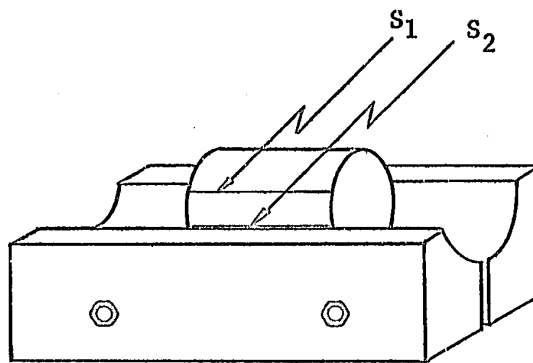
- (a) Schematic diagram showing the methods of obtaining sections of the central fiber at various angles (θ) to a reference line.
- (b) Clamp assembly used to support the specimen during grinding.
- (c) Clamp with specimen in position for grinding.



(a)



(b)



(c)

the set of subgrains was at its position of maximum contrast with respect to the matrix. The angle at this position of the stage was noted, and the structure, termed structure A, was photographed using a Polaroid, series 420 camera. Further rotation of the stage produced a field that was completely dark, though different samples did not produce fields of equivalent darkness.

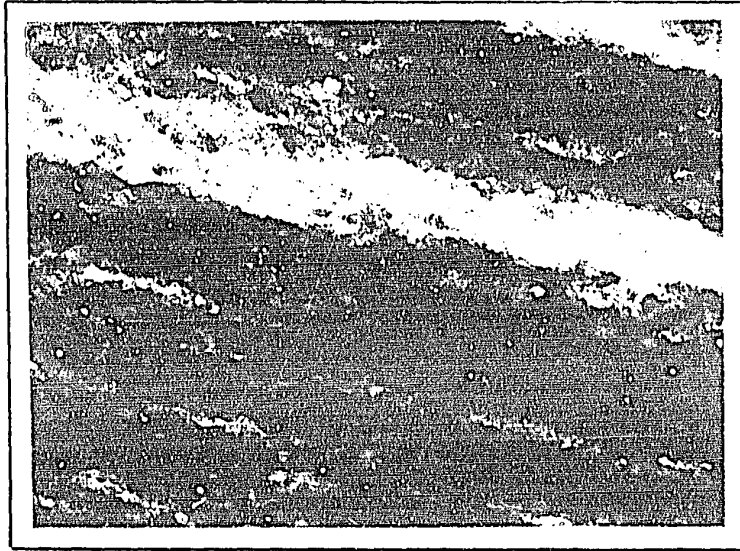
As rotation of the sample was continued, a visible substructure was again encountered. This was called structure B (see Fig. 14). The subgrains that appeared dark or black in structure B, appeared light in structure A, and vice versa for the ones that appeared light in structure B. On further rotation, all the contrast between the subgrains disappeared and the whole field turned white. On continued rotation, contrast between the individual subgrains began to reappear and increase in intensity. The structure that was visible now was again structure A.

It was extremely difficult to determine the point at which the field was lightest; therefore, a note was made of the angle at which all sign of structure disappeared and the angle at which a structure began to reappear. The arithmetic average of these two angles was then used as the angle for a white field. The angles at which the white field, the dark field, structure A, and structure B were observed, were recorded for a 360° rotation of the stage. These readings were used to determine the misorientation between subgrains as discussed in Section 8.3.

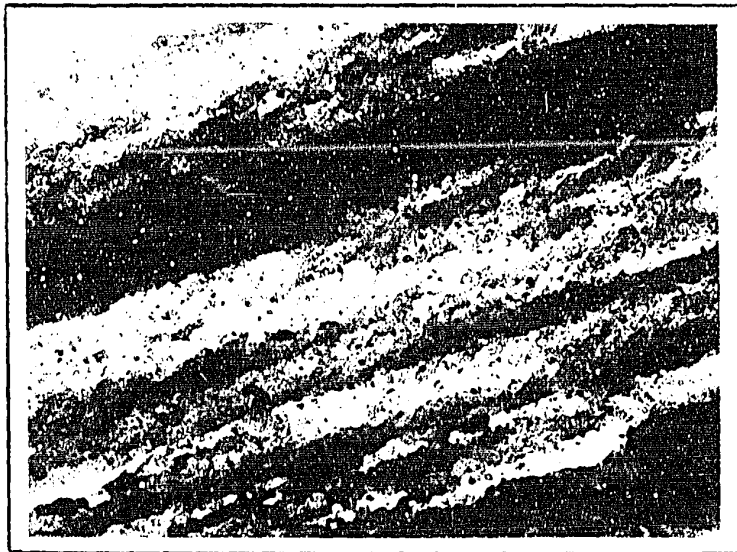
FIGURE 14

Optical micrographs showing appearance of fiber
with the stage set to the position considered as:

- (a) Structure A (Polarized Light 200X)
- (b) Structure B (Polarized Light 200X)



(a)



(b)

4.6 OPTICAL DETERMINATION OF SUBGRAIN SIZE

The subgrain size was determined by random traverses of the samples with a moveable cross-hair in the ocular. The distance of travel of the cross-hair per revolution of the micrometer had previously been calibrated using a microscope stage micrometer. The number of subgrains crossed and the total distance travelled in each traverse were noted. Several traverses were made with the stage at each setting. The stage was then rotated slightly and the procedure was repeated. This was necessary since certain subgrains, which appeared as single entities at a particular setting of the stage, were found to break up into two or more separate subgrains as the stage was rotated slightly. Subgrain size measurements were carried out on each of the two substructures (i.e., A and B) observed on stage rotation. For any one fiber containing detectable subgrains, an average of 300 to 500 subgrains were traversed in order to determine the average subgrain size.

4.7 EFFECT OF VARYING THE OXIDE COATING THICKNESS ON CONTRAST BETWEEN SUBGRAINS

To determine the effect of different thicknesses of coating on the optical appearance of the substructure, a polygonized sample of 1S aluminum and a coarse-grained recrystallized sample of super-purity aluminum were polished and anodized for increasing lengths of time. These were: 30, 60, 90, 120, 150, 180, 240, 480 and 960 seconds. Both samples were anodized for the length of time shown first,

observed under the optical microscope and photographed, and then anodized further to produce the successive accumulative lengths of time. A note was made of the exposure time required for each photograph and of the relative amount of grain or subgrain contrast, as seen in section 5.4.

4.8 OPTICAL EFFECT OF TILTING SAMPLE

The effect of tilting the coarse-grained super-purity sample was determined after a total of 90 seconds of etching. The angles of tilt used were 1°, 2°, 3°, 4°, and 10°. The tilting of the 0.680 inch wide sample for the one or two degree positions was accomplished by the insertion of an appropriate feeler gauge under one side. For the larger angles of tilt, the specimen was raised by the insertion of a suitable wedge under one side. The effect of tilting the sample on the contrast between grains is described in the results.

4.9 TRANSMISSION ELECTRON MICROSCOPY

For examination by transmission electron microscopy, 3/4 inch lengths were cut from the 0.494 inch extrusions and prepared as for optical examination. The fiber of interest was marked by fine scratches at each end of the fiber and the sample was thinned from one side only, the side opposite the one which was observed optically. Thinning was accomplished by first mechanically polishing the sample down to a thin sheet. A disc in the fiber of interest was then jet machined and dished on one side with a water solution of 10% nitric acid at a

voltage of 80 volts. The anodized coating was removed using a 10% NaOH solution. Final thinning was carried out using a solution of 20% perchloric acid in ethanol at a voltage of 12 volts.

The substructure within the chosen fiber was inspected using a JEM - 6A, 100 KV electron microscope following standard thin foil techniques.* The subgrain size was measured by the present author using a technique described by Hilliard (67) and the crystallographic plane of section was determined by electron diffraction, as was the misorientation between subgrains.

4.10 SCANNING ELECTRON MICROSCOPY

The principle of the scanning electron microscope is that a beam of electrons, which is focused to a very small spot, is made to move over the surface of the sample. The electron current leaving the sample is collected and amplified, and is then used to modulate the brightness of a spot on a cathode ray tube which is moving in synchronism with the spot of electrons on the sample. The modulating electron current is not solely dependent upon the electrons emitted by secondary emission from the bombarded surface but is made up in great part of scattered electrons. Electrons are scattered from the surface if the mean plane of the surface under examination is set at an angle of 25° to 45° to the incident beam. Under these conditions,

* Thinning and examination of the specimens by electron microscopy was carried out by Dr. H. J. McQueen of the Ecole Polytechnique.

it is found that the modulating current depends strongly on the angle between the incident beam and the portion of the surface on which the primary electron beam is falling. This angle normally varies considerably from point to point of the surface, so the picture finally built up is related to the topography of the surface, rather than to its secondary emission properties (68). In this manner the topography of the surface may be resolved in great detail, since large magnifications are possible due to the short wavelength of the electrons used.

Representative areas of various samples were examined with a scanning electron microscope*, first after electropolishing and then after electrolytic etching. Each area of interest was investigated at low magnification (approx. 300 X) and then selected areas were photographed at higher magnifications, as required to bring out detail. As the oxide is a dielectric material and becomes charged up in the microscope, it was necessary to coat the surface of the sample with a thin layer (about 100 Å thick) of vacuum deposited gold-palladium alloy (60% Au - 40% Pd).

* The scanning electron microscopy was performed by Mr. A. Rezanowich of the Pulp and Paper Research Institute of Canada.

CHAPTER FIVE

RESULTS OF OPTICAL METALLOGRAPHY

5.1 TYPES OF SUBSTRUCTURES OBSERVED

When a rod of polygonized aluminum was sectioned longitudinally and anodically etched, as described in Section 4.3, a variety of apparent substructures could be seen under polarized light. These can be divided into four general categories which are illustrated in Fig. 15. The categories are:

- a) an equiaxed, well-defined substructure (Fig. 15a)
- b) a definitely cross-hatched substructure (Fig. 15b)
- c) an indefinitely cross-hatched substructure (Fig. 15c)
- d) no substructure (Fig. 15d).

The categories are by no means distinct groups but represent portions of a continuous spectrum, beginning with a very clear equiaxed substructure at one end and ending with one in which no substructure whatever can be seen under the optical microscope. The cross-section of an extruded rod can contain all four types of structure simultaneously, though the major part of the sections was usually cross-hatched.

The average grain size, as determined optically, ranged from about 9 to 13 microns. There was little contrast, in most cases, between the subgrains in a particular fiber, while the contrast between adjacent fibers was usually very striking. This indicated that there were large misorientations between the subgrains in adjacent fibers when they were sectioned longitudinally.

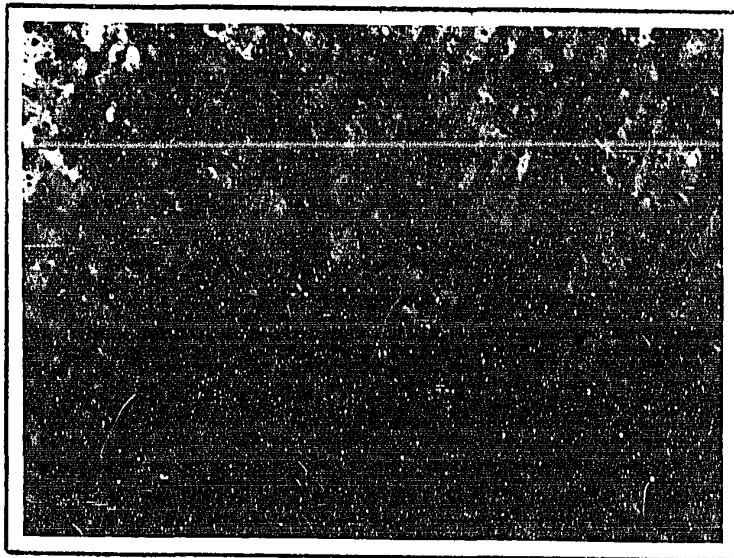
Very little contrast was evident, on the other hand, when transverse sections of extruded rod were examined, and it was difficult to distinguish between subgrains and between adjacent fibers, as illus-

FIGURE 15

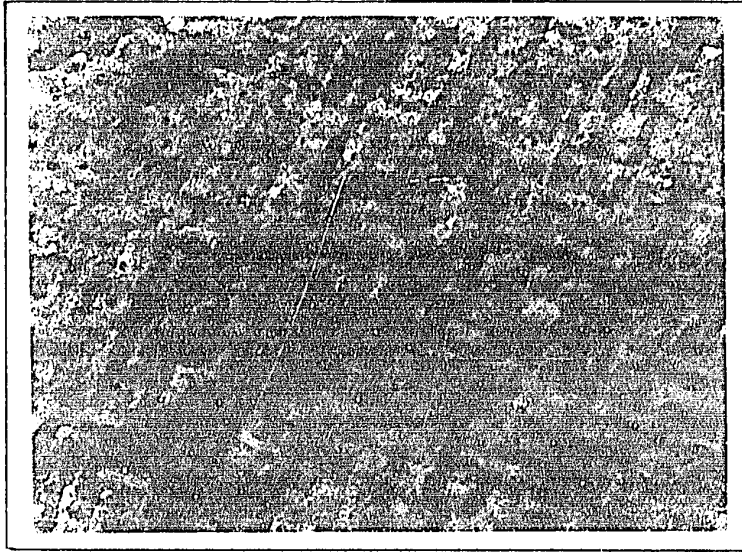
- (a) Optical micrograph of equiaxed substructure.
(Longitudinal section, polarized light 200X.)
- (b) Optical micrograph of a "definitely cross-hatched" substructure.
(Longitudinal section, polarized light 200X.)
- (c) Optical micrograph of an "indefinitely cross-hatched" substructure.
(Longitudinal section, polarized light 200X.)
- (d) Transverse section of an extruded rod, showing that no substructure is visible, and that individual fibers are indistinguishable in most cases.
(Polarized light 200X.)



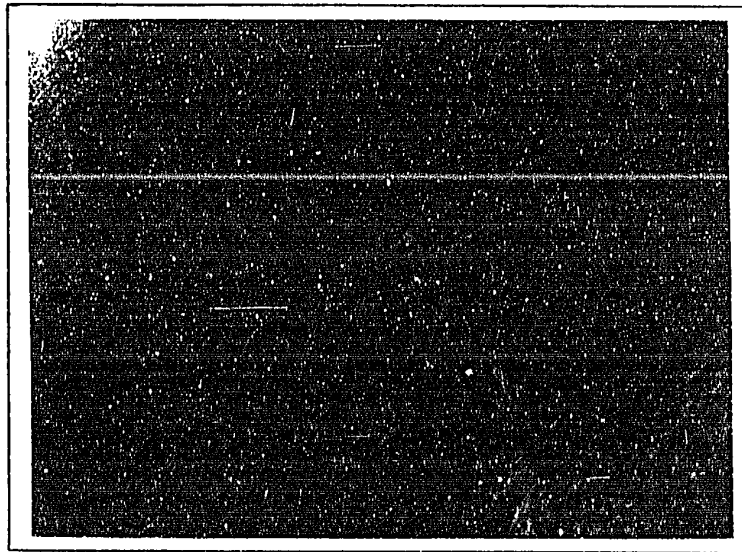
(a)



(b)



(c)



(d)

trated in Fig. 15d. The reasons for the difference between the longitudinal and transverse microstructures will be dealt with in the Discussion.

5.2 TYPES OF SUBSTRUCTURES OBTAINED ON SECTIONING SELECTED FIBERS AT DIFFERENT ANGLES

Central fibers were sectioned, as described previously, at the following angles to a longitudinal reference line: 30° , 45° , 60° , 90° , 120° , 135° and 150° . The types of substructure obtained from each set of sections are summarized in Table II. The substructures found in Set No. 3, which cover the whole range of substructures observed, are shown in Fig. 16. Note that the subgrain size was different for each angle of section, as shown in Table III.

TABLE II
SUBSTRUCTURES OBTAINED ON SECTIONING
FIBERS AT DIFFERENT ANGLES

SET No. 1

0	equiaxed, well-defined
45	faintly cross-hatched
90	faintly cross-hatched, almost equiaxed
135	mostly equiaxed

SET No. 2

0	faintly cross-hatched, almost equiaxed
30	equiaxed, though not very definitely
60	large equiaxed
90	very indefinitely cross-hatched, almost no structure
120	definitely cross-hatched
150	indefinitely cross-hatched, very faint

SET No. 3

0	definitely cross-hatched
30	definitely equiaxed
60	indefinitely cross-hatched, verging on no structure
90	equiaxed, verging on cross-hatched
120	equiaxed, very large
150	equiaxed

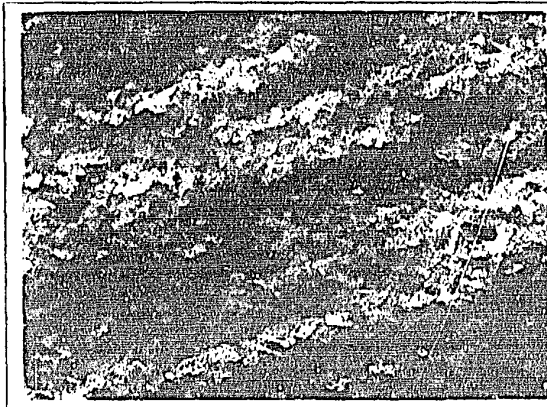
TABLE III
SUBGRAIN SIZES FOR SET NO. 3

<u>Angle of Section</u>	<u>Average Subgrain Size* (microns)</u>
0°	9.9
30°	10.0
60°	10.1
90°	10.1
120°	12.4
150°	11.4

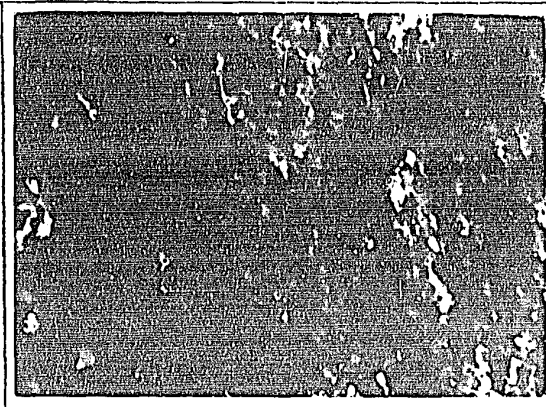
* Average for 300 to 500 subgrains.

FIGURE 16

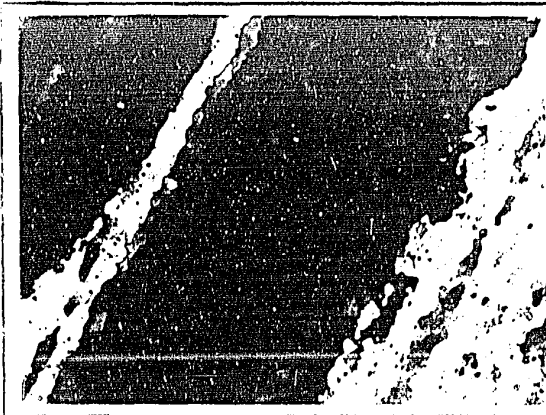
Sequence of substructures observed when one fiber was sectioned longitudinally at different angles to a plane of reference. Polarized light (150X).



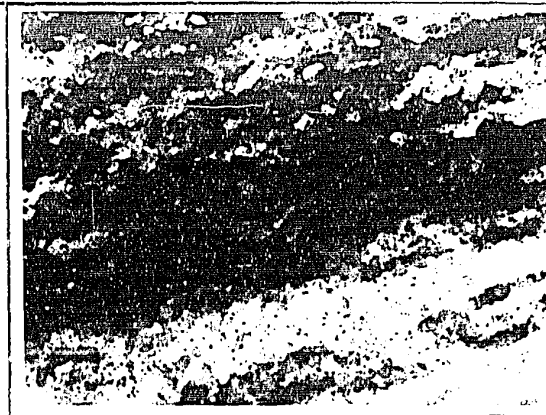
0°



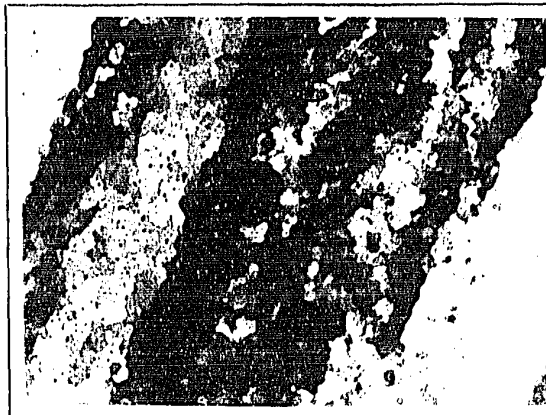
30°



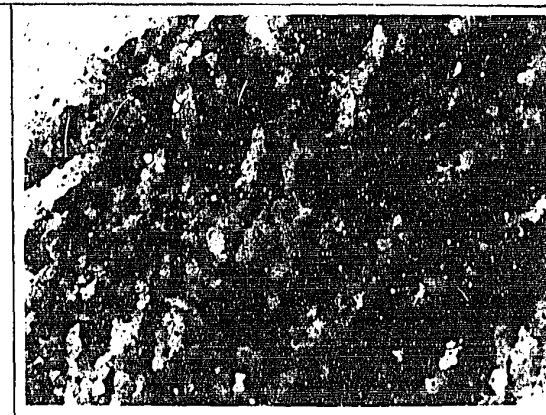
60°



90°



120°



150°

5.3 MISORIENTATION BETWEEN SUBGRAINS

Attempts to measure the misorientation between adjacent subgrains by means of stage rotation were found to give inconsistent results.* It was found that the amount of stage rotation required to bring adjacent subgrains alternately to the same shade of grey or darkness depended on the direction of rotation and on the actual shade of grey chosen for comparison. In addition to this, it was extremely difficult to determine when a subgrain was at its position of maximum darkness, if this was chosen as the point of reference. If a particular shade of grey was chosen rather than that of maximum darkness, it was difficult to determine when the second subgrain reached the

* Orientation is defined as the angular relationship between a crystal or molecular alignment and a set of external reference directions. The orientation difference or misorientation between two crystal lattices can be described in a number of ways.

One such way is to consider the misorientation as a combination of a pure tilt and a pure twist misorientation. These describe, respectively, a rotation about a common axis in the plane of the boundary, and a rotation about an axis perpendicular to the boundary.

A second way is to describe the misorientation in terms of three orthogonal rotations about a set of co-ordinate axes. These rotations can be combined to obtain one rotation about the axis of a common crystallographic direction, though three parameters are still required to define a misorientation in this way. These parameters are the following: two to describe the axis about which rotation takes place and one to describe the amount of rotation about this axis. A method to determine the orientation of the common axis and the amount of rotation about it, when the orientations of the two grains are known, was presented by Liu (76) in 1964.

When a section is made through a grain boundary, a two-dimensional view is obtained in which only a component of the misorientation is observed. This component may be smaller or equal to the true misorientation, depending on the plane of section.

identical shade of grey that the first one had before it was moved. The error involved in this technique was quite large compared with the value of misorientation and so it was abandoned.

It was observed, however, that at particular settings of the microscope stage, the subgrains within a given fiber could be divided into two groups. The two groups differed in shade from each other and the subgrains in each group were of about the same shade. Usually, when one group was dark, the other was light, and vice versa. Structure A was the name given to the structure obtained when one group was at its position of maximum darkness, and this also corresponded to the condition of maximum contrast between it and the group of the opposite shade. Structure B was the term applied to the condition for which the subgrains that appeared light in structure A were at their position of maximum darkness instead. Structure A and Structure B for a particular specimen are illustrated in Fig. 14.

The amount of stage rotation observed between structure A and structure B is an indication of the average misorientation between the subgrains in the two groups. That is, it is an indication of the maximum optical misorientation present within a single fiber. The results of readings obtained by this method are listed in Table IV, and will be further interpreted and discussed in Section 8.3.

TABLE IV

MISORIENTATION READINGS BY OPTICAL STAGE ROTATION

Test No.	White Field to Structure A (degrees)	Structure A to Dark Field (degrees)	Dark Field to Structure B (degrees)	Structure B to White Field (degrees)	White Field to White Field Rotation (degrees)	Structure A across Dark Field to Structure B (degrees)	Structure B across White Field to Structure A (degrees)	Dark Field across Structure A to White Field (degrees)	White Field across Structure B to Dark Field (degrees)
3-1	34.1	8.3	6.8	41.9	91.1	15.5	77.2	42.2	48.5
3-2	34.3	7.4	8.8	39.6	90.1	16.1	73.9	41.4	48.3
3-3	38.7	5.0	5.4	40.9	90.0	10.4	79.6	43.7	46.3
3-4	31.3	15.3	7.9	35.8	90.3	23.3	66.8	46.3	43.7
3-5	39.9	7.5	11.1	30.5	89.0	18.6	70.4	47.4	41.6
3-6	36.6	12.8	12.1	28.6	90.1	24.9	65.1	49.3	40.7
AVG.	35.8	9.4	8.7	36.2	90.1	18.1	72.0	45.1	44.8
3-7	39.9	6.0	5.7	38.5	90.1	11.7	78.4	45.9	44.2
9-1	39.8	4.6	5.0	40.5	89.9	9.6	80.3	44.5	45.5
9-2	35.6	8.7	7.8	37.3	89.4	16.5	72.8	44.3	45.0
AVG.	38.7	6.4	6.2	38.8	90.1	12.6	77.2	44.9	44.9

Each angle given in this table is the average of four readings. The scatter of the readings about the average was approximately $\pm 2 - 3^\circ$.

5.4 THICKNESS OF OXIDE COATING

It was found that increasing the thickness of the oxide on the aluminum, while holding the incident light intensity constant, resulted in an increase in the ellipticity of the light reflected from the surface of the specimen. The relative intensity of the rotated light was estimated from the time required to expose a photograph to a given degree. The results of this study are shown in Table V, and some representative photographs are presented in Fig. 17.

TABLE V
EFFECT OF OXIDE THICKNESS ON REFLECTION OF LIGHT

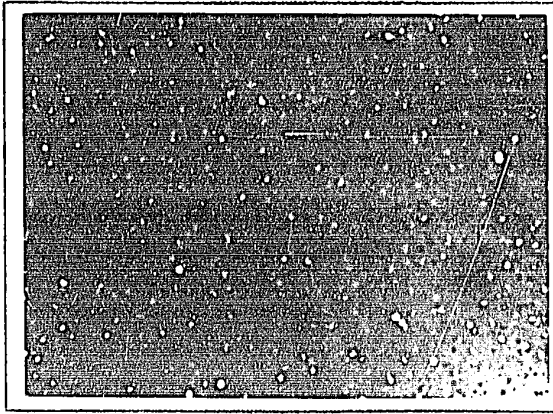
<u>Total Time of Etch (sec.)</u>	<u>Subgrain Sample Exposure Time (sec.)</u>	<u>Large Recrystallized Sample Exposure Time (sec.)</u>
30	120	30
45	60	15
60	60	
90	30	2
120	15	
150	5	
180	5	
210	5	
240	5	2
480	1	
960	0.5	5

It was also found that after a certain amount of overanodizing, the subgrain boundaries become less well defined and the contrast between adjacent subgrains began to disappear. As the topography of the oxide surface changes with etching time (42), this indicated that the loss of contrast between adjacent subgrains was probably

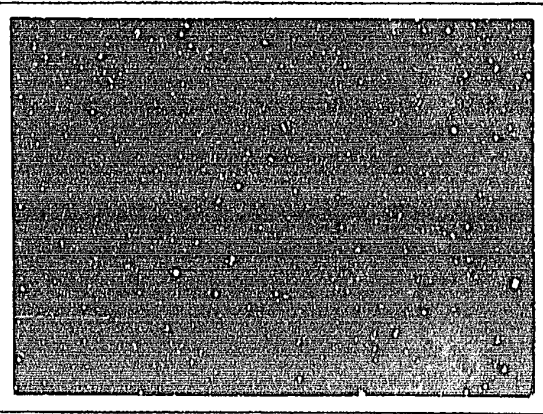
FIGURE 17

Sequence of micrographs illustrating the changes in the definition of the substructure with increasing thickness of oxide.

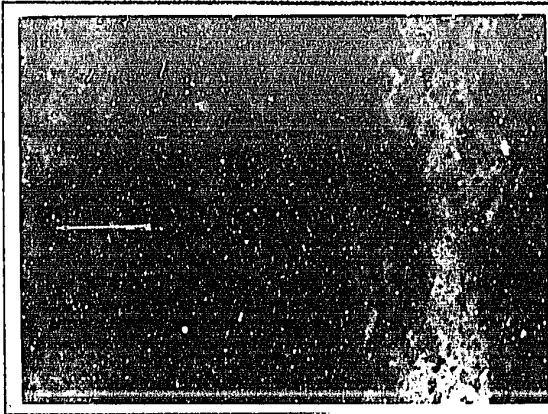
- | | |
|-------------------|-------------------|
| (a) 30 sec. etch | (d) 150 sec. etch |
| (b) 60 sec. etch | (e) 240 sec. etch |
| (c) 120 sec. etch | (f) 960 sec. etch |



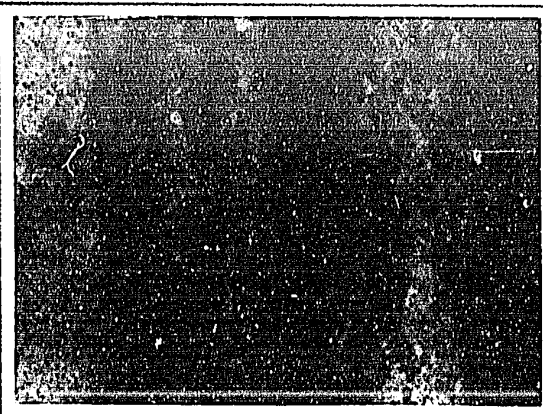
(a)



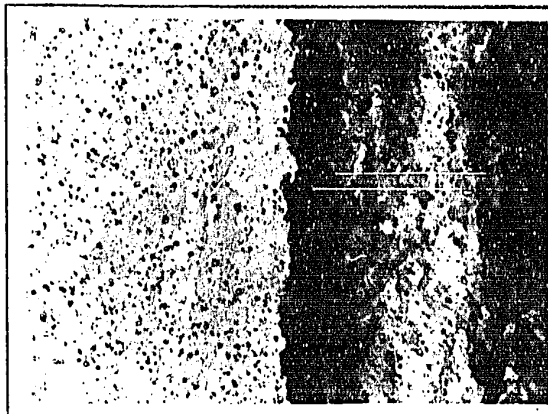
(b)



(c)



(d)



(e)



(f)

associated with changes in furrow structure.

5.5 EFFECT OF CHANGING THE ANGLE OF TILT

To obtain further data on the mechanism of reflection of the incident light from the oxide surface, the specimen surface was tilted at small angles with respect to its usual horizontal position. It was found that on a recrystallized sample in which the grain size was very large, increasing the angle of tilt from 0° to 3° increased the contrast between adjacent grains, as seen in Fig, 18. Increasing the angle of tilt still further to 4° produced no change in contrast, while at 10° there was almost no contrast left between the adjacent grains. The exposure time required at 10° of tilt was considerably greater than that for the small tilt angles. This can be attributed to the fact that there was a considerable amount of light lost by reflection away from the microscope axis.

5.6 EFFECT OF USING LIGHT OF DIFFERENT WAVELENGTHS

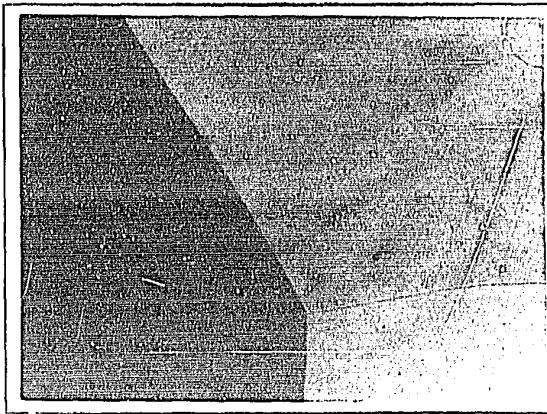
When a polygonized sample was examined with light which had passed through a blue filter, (Wratten No. C-49), it showed considerably more contrast than when viewed using light that had passed through a red filter (Wratten No. F-Bd8). Setting aside differences in red and blue sensitivity in the observer, this indicated that the mechanism of contrast production operated more effectively with light of short wavelength. The effect may possibly be ascribed to the fact that the furrow spacings and slope lengths are in the same range of

FIGURE 18

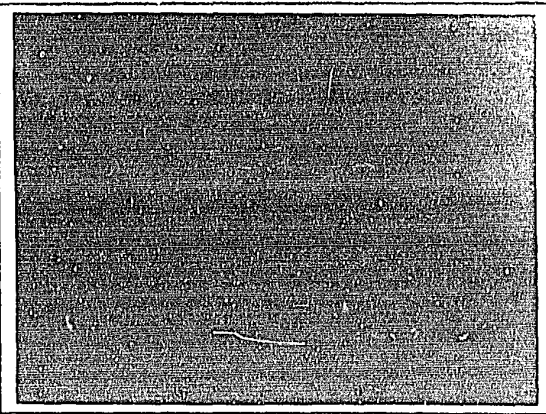
Variation in contrast between three large recrystallized grains with different angles of tilt of the sample from the normal horizontal position.

- | | |
|--------------|-------------------|
| (a) 0° tilt | 2 sec. exposure |
| (b) 1° tilt | 2 sec. exposure |
| (c) 2° tilt | 15 sec. exposure |
| (d) 3° tilt | 15 sec. exposure |
| (e) 4° tilt | 15 sec. exposure |
| (f) 10° tilt | 240 sec. exposure |

Polarized light (200X).



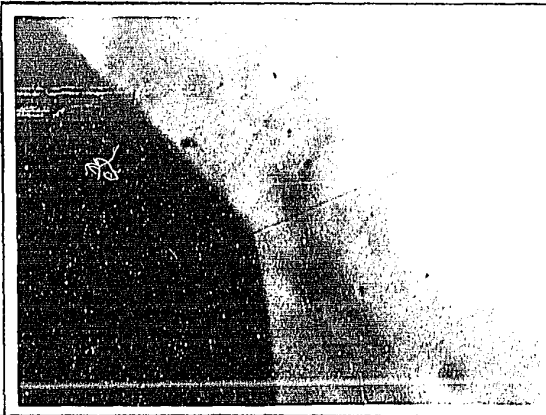
(a)



(b)



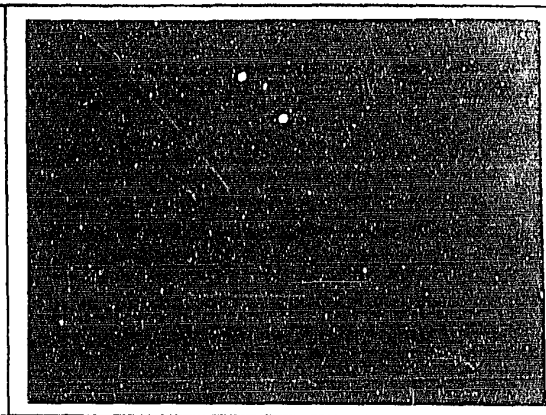
(c)



(d)



(e)



(f)

magnitudes as the wavelength of light.

When white light was used and a sensitive tint plate inserted into the optical train, the following results were obtained:

- 1) It was extremely difficult, if at all possible, to distinguish the separate subgrains.
- 2) The bands of similarly oriented subgrains were easily distinguishable and adjacent bands appeared in complementary colors such as red-pink and blue-green.

5.7 REFLECTION FROM PARALLEL SCRATCHES ON ALUMINUM SURFACE

Opposing theories concerning the production of contrast between grains are based either on reflection from the furrowed surface of the oxide, or transmission through the optically anisotropic oxide and reflection at the smooth oxide/metal interface. The question of whether reflection from the furrowed surface alone could be responsible for subgrain contrast was further investigated as follows:

A specimen of aluminum, which is optically isotropic, was hand polished up to 4-0's emery paper. Care was taken to make certain that on the last few passes, the scratches on the surface were parallel and as regular as possible. Another set of scratches was made at approximately 45° to this direction, in an adjoining part of the specimen. When this sample was inspected using plane polarized light, it was found that extinction occurred when the scratches were either perpendicular or parallel to the plane of polarization of the incident light. When the scratches were at other angles, the surface varied

in brightness, with maximum brightness being produced when the scratches were inclined at 45° to the plane of the polarizer or analyser.

This indicated that reflection from a furrowed surface alone could produce elliptically polarized light and that the presence of such light is not necessarily indicative of anisotropic properties in the reflecting material.

5.8 REFLECTION FROM FURROWS ON OVERANODIZED COARSE-GRAINED SAMPLE

To determine whether the furrows on the oxide surface were involved in a similar effect, a highly overanodized coarse-grained sample, in which the furrow directions were clearly visible, was used to determine the orientation of the furrows at extinction. It was found that each grain appeared darkest when its furrows were either perpendicular or parallel to the incident plane of polarization. Also, maximum brightness occurred at 45° , as was seen previously with the metal surface. The results of this test on oxide furrows thus agreed fully with those of the previous section on metal scratches.

5.9 REFLECTION AFTER APPLYING A METAL COATING ON THE OXIDE

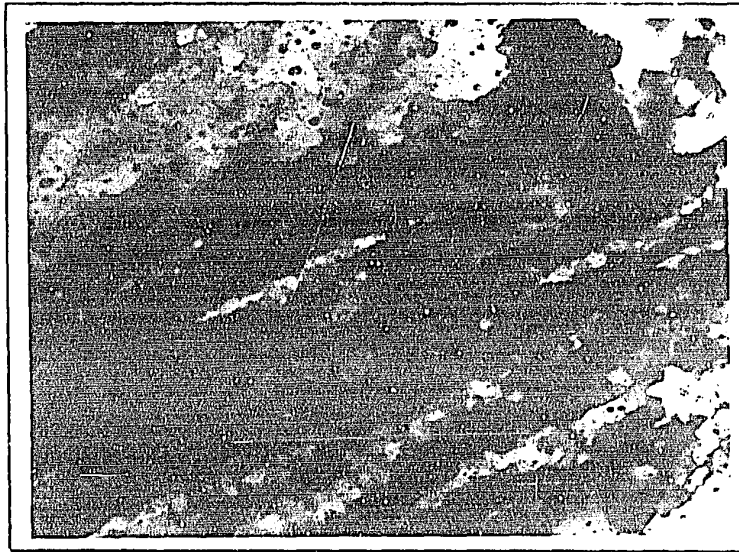
A set of samples was prepared following the usual technique for optical observation. Representative areas of each type of sub-structure were photographed, as seen in Fig. 19a. A selected sample was then coated with a thin film (about 400 \AA) of gold-palladium

FIGURE 19

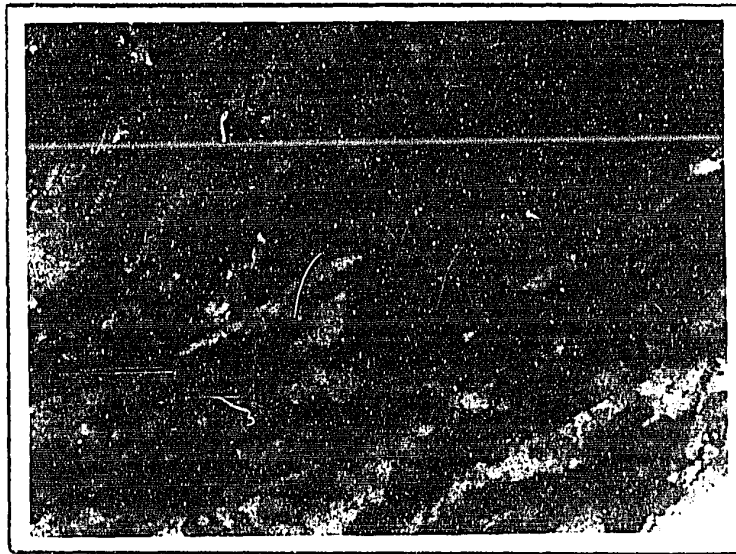
Appearance and clarity of definition of substructure:

- (a) after anodic etching;
- (b) after anodic etching and vacuum deposition of
400 Å thick coating Au-Pd alloy.

Polarized light (200X).



(a)



(b)

alloy (60% Au - 40% Pd) by standard vacuum deposition techniques, The thickness of the deposited material was great enough to make it opaque to light. This sample was then rephotographed, and part of it is shown in Fig. 19b.

It can be seen that the same substructure is observed after coating with gold-palladium, though the relative contrast is somewhat decreased, and the total intensity is considerably less. This shows that the ellipticity of the reflected light was somewhat decreased by the addition of the coating.

The results of this test showed conclusively that when plane polarized light is reflected from the surface of an anodized aluminum specimen, the reflected light is elliptically polarized, and that this is due primarily to the furrowed topography of the oxide surface and not to the optical anisotropy of the aluminum oxide. The decrease in the intensity of the reflected light after deposition of the opaque metal probably resulted from the alteration of the furrow shape, and so of the reflecting surface. Also, the p and s reflectivities of the metal are different from those of the aluminum oxide which it supplanted as the reflecting medium.

CHAPTER SIX

TRANSMISSION ELECTRON

METALLOGRAPHY RESULTS

6.1 STRUCTURE

The different substructures observed on the optical microscope level could not be distinguished from each other on the transmission electron microscope level. In the latter case, equiaxed subgrains were always observed with fairly well-formed dislocation boundaries. The boundaries were narrow, did not show thick dislocation tangles, and the subgrain interiors were relatively dislocation free. The subgrains in each sample did not show any evidence of cold work, were not elongated, and were similar in many respects to those produced by annealing after cold work.

Representative electron micrographs corresponding to three of the main types of optical substructures are shown in Fig. 20. The average size of the subgrains ranged from 7.7 to 9.0 microns, as shown below:

equiaxed substructure	7.7 microns
definitely cross-hatched	7.7 microns
indefinitely cross-hatched	9.0 microns

6.2 ORIENTATIONS AND MISORIENTATIONS

The misorientations between the subgrains on the dislocation level were found by electron diffraction. The general procedure was to determine the orientation of several adjacent subgrains in a particular area, and then to find the orientation of one or two subgrains at a distance of several subgrains from the original area. It was found that the misorientation between adjacent subgrains was usually

FIGURE 20

Representative transmission electron micrographs of the subgrains in the following optical substructures:

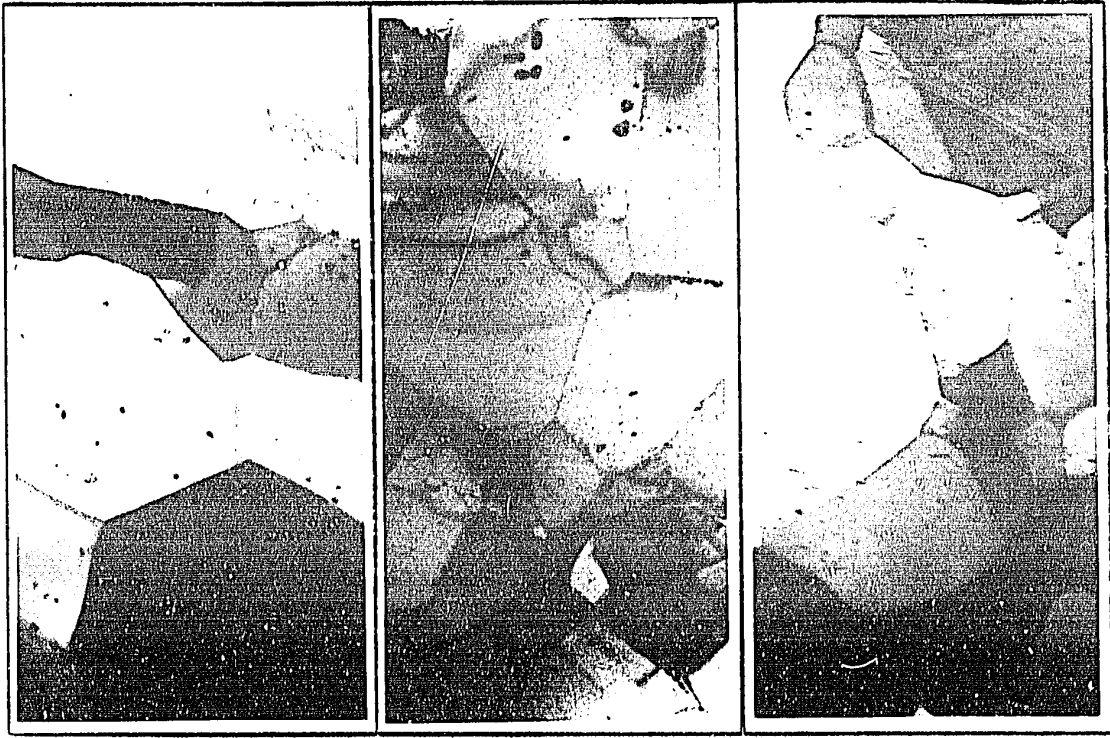
- (a) equiaxed
- (b) definitely cross-hatched
- (c) indefinitely cross-hatched.

(Each at 2000X).

FIGURE 21

Electron diffraction patterns obtained from samples that appeared:

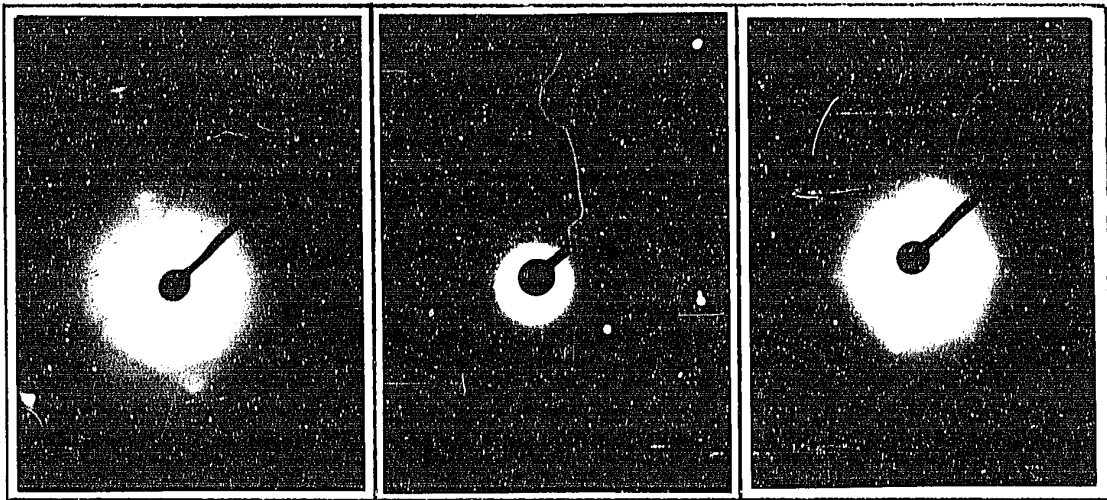
- (a) equiaxed
- (b) definitely cross-hatched
- (c) indefinitely cross-hatched.



(a)

(b)

(c)



(a)

(b)

(c)

small, of the order of minutes or one or two degrees, while the orientations of the distant subgrains differed by 6° to 8° from those of the adjacent ones.

It was also found that the misorientations along a given direction in a subgrain field were not additive. That is, where the average misorientation between ten subgrains along a straight line was say 3° , the misorientation between the first and the last subgrain was always considerably less than 30° . Several such sequences of misorientation were measured for linear distances of the order of 20 to 25 microns. It should also be pointed out that in no case was a misorientation between adjacent subgrains larger than 6° found; furthermore, no high angle boundaries were ever observed in the subgrain regions.

Electron diffraction was also used to determine the plane of section corresponding to three of the optical structures observed. The results are summarized in Table VI and representative diffraction patterns are displayed in Fig. 21.

TABLE VI

PLANE OF SECTION AND AVERAGE MISORIENTATION
FOR DIFFERENT OPTICAL SUBSTRUCTURES

<u>Optical Structure</u>	<u>Plane of Section</u>	<u>Average Misorientation</u>
equiaxed	(310), (210)	$4^\circ 30'$
definitely cross-hatched	(110)	$4^\circ 34'$
indefinitely cross-hatched	(110)	$3^\circ 49'$

6.3 REPLICAS OF OXIDE COATING

It was observed optically that no substructure (or at most a faint hint of substructure) was apparent on etched transverse sections, whereas easily visible substructures were found on the longitudinal sections. In order to determine the reason for this difference, plastic replicas of transverse and longitudinal etched surfaces were investigated by electron microscopy. It was found that longitudinal replicas showed slight differences in elevation between bands or regions of subgrains, and revealed a distinct furrow structure in each subgrain. In many cases, there was a slight difference in furrow direction between adjacent subgrains, while in some cases no such change of direction was observed, as can be seen from Fig. 22a.

On examining the transverse replicas, no furrow structure was observed and the etched surfaces were seen to be somewhat speckled. The subgrain boundaries were delineated by small ridges which probably were not large enough to be observed optically. Periodically, there appeared to be a difference in elevation between adjacent subgrains, as can be seen from Fig. 22b. It is possible that these differences in elevation are responsible for the substructure which can be detected optically using phase contrast.

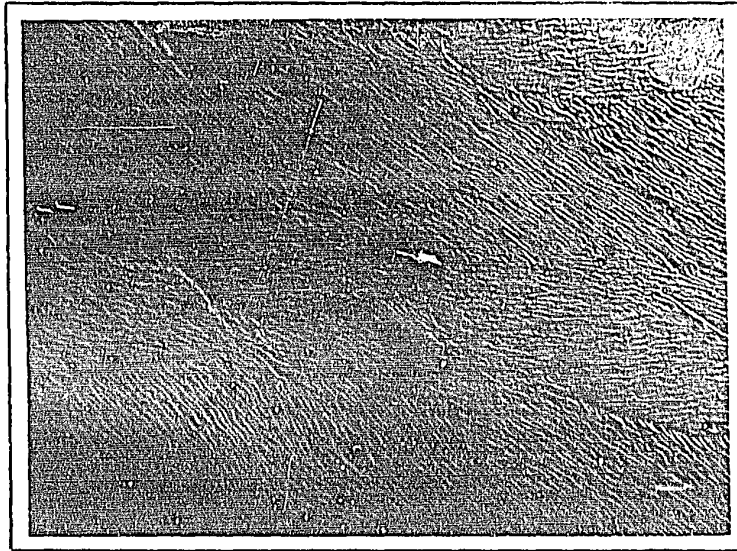
In order to extend the results obtained from the use of replicas with the conventional electron microscope, the topography of the oxide surface was further studied with a scanning electron microscope. A selected sample was first inspected after electro-

FIGURE 22

Plastic replica micrographs of:

- (a) Longitudinal section where a substructure was visible;
- (b) Transverse cross-section where no substructure was visible.

(Each 1500X).



(a)



(b)

polishing and before electrolytic etching. In this case, the surface was flat with no sign of furrows, ridges, speckles or any other surface imperfections, even at magnifications as high as 25,000 X. After anodizing, representative areas of the equiaxed, definitely and indefinitely cross-hatched substructures were investigated.

CHAPTER SEVEN

RESULTS OF SCANNING

ELECTRON METALLOGRAPHY

7.1 EQUIAXED SUBSTRUCTURE

Under the scanning electron microscope, the topography of an equiaxed region has the appearance shown in Fig. 23. It can be seen that the furrows are not perfectly parallel, and that the furrow directions change from subgrain to subgrain. In any one subgrain, the furrow direction is generally constant, though some deviations can be seen at the ends of some of the furrows. It can also be seen that the furrow density is relatively constant within individual subgrains.

Note that the average size of the regions denoted by similar furrow directions is in agreement with the average subgrain size observed optically and that the misorientation between furrow directions in adjacent subgrains coincides with the values obtained by optical methods.

7.2 DEFINITELY CROSS-HATCHED SUBSTRUCTURE

In the areas that had this type of optical substructure, two types of furrow structure could be observed:

- a) either all the furrow directions were uniform,
as in Fig. 24a, or
- b) a herringbone pattern was observed, as in Fig. 24b.

In case a), although the general furrow direction was constant over the entire fiber inspected, it can be seen that the density of the furrows varies from location to location. Moreover, the size of these "patches" of furrows agrees very well with the

FIGURE 23

Scanning electron micrograph of the oxide surface corresponding to the equiaxed substructure. Note variation in furrow direction between adjacent regions. (1000X)

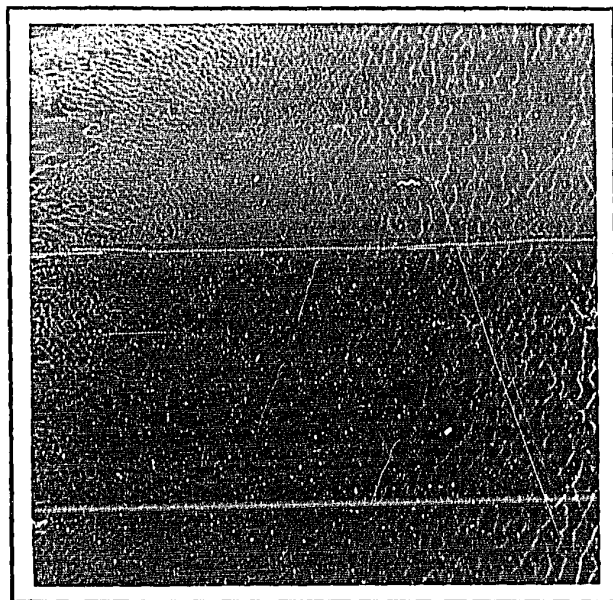
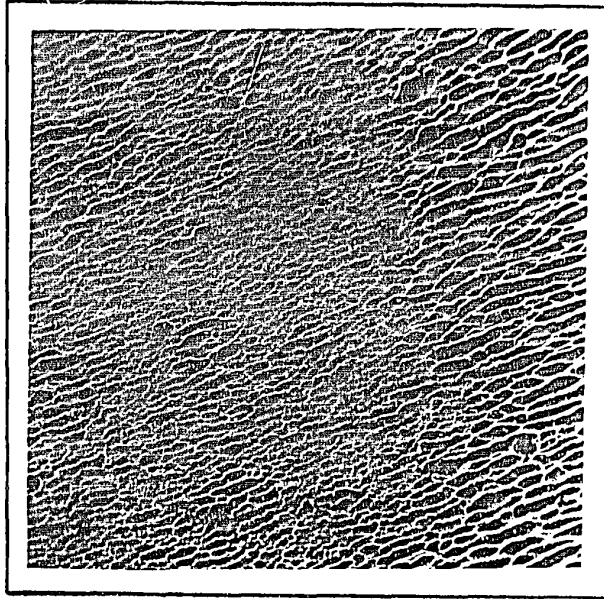


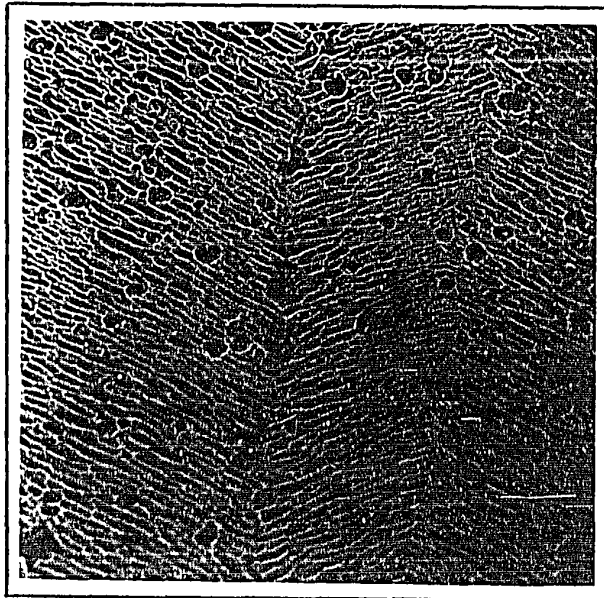
FIGURE 24

Scanning electron micrographs corresponding to definitely cross-hatched regions:

- (a) showing region where furrow direction is uniform; (1300X)
- (b) showing region where a "herringbone" pattern exists. (700X)



(a)



(b)

size of "subgrains" or cross-hatching observed on optical inspection.

From Fig. 25 it can be seen that in regions of different furrow density, the slopes of the furrows are different. In regions of closely arranged furrows, the slopes of the grooves are considerably steeper than those of furrows that are arranged less densely. It can also be seen that the depth of each of the furrows is approximately the same.

In case b), it can be seen that there is both a difference in orientation of the furrows and also a difference in the density of furrows from region to region. The difference in furrow orientation along this herringbone pattern is of the order of 30° to 40° .

7.3 INDEFINITELY CROSS-HATCHED SUBSTRUCTURE

A typical example of an indefinitely cross-hatched area is shown in Fig. 26. Here it can be noticed that no definite furrow structure exists, but that an oxide film of relatively uniform thickness persists over the whole area. A hint of a furrow structure is seen, and periodically large depressions are noticed. The "ghost" furrow structure is unidirectional over areas that are considerably larger than the pattern size observed optically; moreover, the angle between the furrow directions in adjacent regions is relatively large. Therefore, it is improbable that the "ghost" furrow structure produces the optical effect. Instead, the periodic large depressions, which also have some directionality, are more likely to be responsible for the appearance of indefinite cross-hatching on the optical

FIGURE 25

Scanning electron micrograph illustrating that differences in furrow slope are associated with differences in furrow density.

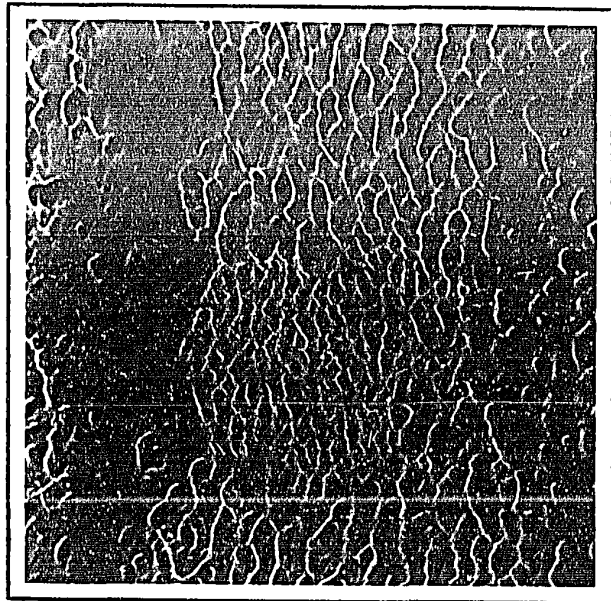
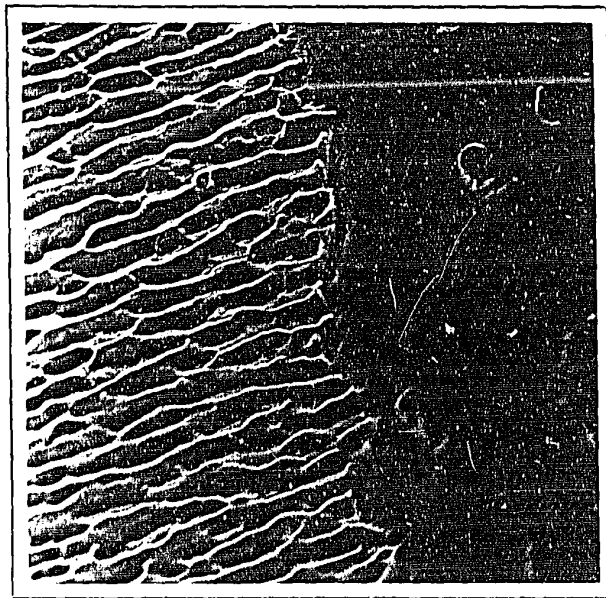
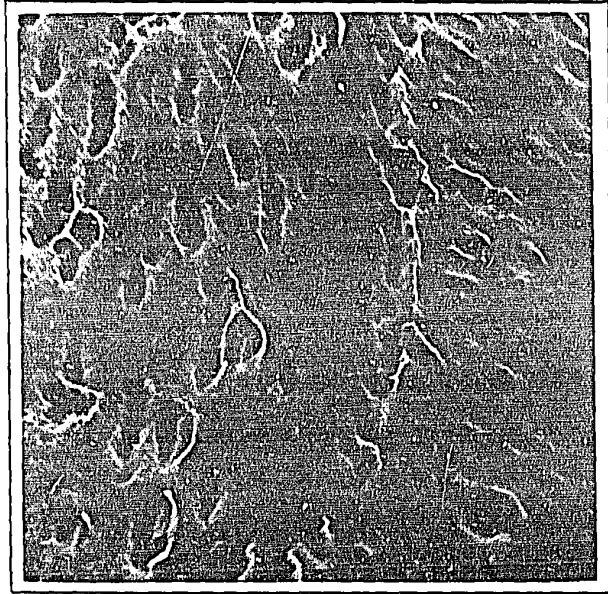


FIGURE 26

Scanning electron micrograph corresponding to an indefinitely cross-hatched region. (1800X)

FIGURE 27

Scanning electron micrograph showing the boundary between a furrowed and a non-furrowed surface (at right). The non-furrowed oxide is of approximately the same thickness as the oxide at the furrow crest.



level. Fig. 27 shows that in regions of this nature, the oxide film thickness is about equal to the maximum oxide film thickness in the furrowed regions.

CHAPTER EIGHT

DISCUSSION

In the procedure used to reveal the substructure of the polygonized aluminum, an anodizing etch was used after electrolytic polishing. The effect of the etch was to build up a layer of oxide on the surface of the aluminum. The irregular topography of the oxide acts on incident plane polarized light so as to produce elliptically polarized light on reflection. The elliptically polarized light, which varies in intensity and azimuth from region to region, causes differently shaded areas to appear in the field of the optical metallograph.

In order to determine the relationship between the patterns observed optically and the actual substructure of the metal, it is necessary to consider the phenomenon from two points of view. First, there is the question of the relation between the structure of the oxide and the orientation of the metal substrate. The second question concerns the mechanism by which the oxide layer converts the incident plane polarized light into reflected elliptically polarized light.

These two questions will now be examined in turn, and the significance of the results described above will be evaluated.

8.1 OXIDE NUCLEATION AND GROWTH

It has been stated above (Section 2.3) that the oxide layer which forms during the anodic etching of aluminum consists of two parts. The one nearer the metal, the barrier layer, is known to be amorphous, and of a thickness which depends on the potential

difference between the metal surface and the electrolyte. It is also known that the potential of the metal is not identical at every point on its surface. The location at which a grain boundary meets the surface is usually at a somewhat lower potential than the grain face itself. This is due to the greater density of vacancies at the grain boundary and involves the ease of electron mobility through such an area (69, 70, 71). As a result of the difference in potential between the grain faces and the grain or subgrain boundaries, the thickness of the barrier layer is slightly less along the boundaries. According to Keller (35), these depressions in the inner amorphous layer act as nucleation sites for the outer crystalline layer.

It further seems likely that the cells of the outer oxide layer nucleate in different orientations with respect to the inner amorphous layer for different forms of discontinuities in the inner layer, although this has not yet been experimentally verified in detail. Once the original nucleus has been formed, as anodizing progresses, it has been shown (35) that additional cells follow the orientation of the originally nucleated cell. Thus regions are formed in which the oxide cell orientation is uniform, and in which the cell orientation differs from that of neighbouring regions.

As the process of growth progresses, single rows of cells form along both sides of the subgrain boundaries, thus delineating the boundaries (35). Continued anodizing results in the formation of additional rows of cells within the subgrains. The rows of cells lead to the furrow structure that can be observed on the surface of the specimens (47). This picture of furrow formation is in agreement

with the scanning electron micrographs and plastic replica results obtained by the present author.

The experiments performed by this author also support a loose relationship between the oxide topography and the plane of section of the specimen. On the other hand, it has also been found that certain discrepancies exist between the subgrain sizes determined optically, and those found by transmission electron microscopy. Furthermore, the values of misorientation obtained optically differ considerably from the values obtained by electron diffraction.

Considering that the true substructure of the material is revealed by electron microscopy, the extent to which the apparent substructures observed optically are reliable, and the manner in which the apparent subgrain misorientations and sizes are related to the true ones remain to be explained. This will be done in two sections, dealing first with furrow orientation and then with size of regions of uniform furrow orientation.

8.2 FURROW ORIENTATION AND METAL SUBSTRATE CRYSTALLOGRAPHY

It has been stated above that the outer oxide layer nucleates first along irregularities in the barrier layer. It is probable that nucleation does not take place simultaneously along the entire length of each sub-boundary, but rather that it occurs at various points along the sub-boundaries, where nucleation is easiest. For this reason, each subgrain is not necessarily delineated by a single set of furrows. It has also been stated that on

further growth of the oxide, additional rows of cells are formed within the subgrains. Thus the amorphous layer exerts no direct influence on the orientation of the cells, nor does the metal substrate, due to the presence of the amorphous layer.

The direction of growth of the oxide cells is governed instead by the details of the irregularities in the amorphous surface at the sub-boundary, and so, only loosely by the nature of the discontinuity in the lattice of the substrate. This is to say that the sub-boundary between adjacent subgrains, when exposed by the $\{100\}$ plane of section, for example, will produce a different effect upon the amorphous layer, than when exposed by the $\{210\}$ plane of section. Thus the latter plane of section can lead to oxide cells being nucleated in somewhat different arrangements than the former plane of section. When further rows of cells are grown, i.e. further furrows formed, their direction and density simply depends upon the arrangement of the originally nucleated cells.

According to this picture, different planes of section can lead to different orientations of oxide cells, but the relationship is not a unique one because the crystallography of the sectioned surfaces does not affect the porous oxide directly, but only through its effect on the topography of the barrier layer at the sub-boundary. The fact that different crystallographic planes can be associated with differences in ease of furrow formation or oxide build-up has in fact been confirmed by Herenguel and LeLong (72).

8.3 RELATION OF SIZE OF REGIONS OF UNIFORM FURROW ORIENTATION TO METAL SUBSTRATE

The size of the subgrains observed optically depends upon the area over which a given furrow direction and density persist. If the nucleation and growth mechanism described above is correct, then it is reasonable that no simple correlation should exist between the subgrain size observed optically and the subgrain size on the dislocation level. A 1:1 relationship between the optical and electron microscope sizes can be expected only when all boundaries and sub-boundaries lead to discontinuities in the furrow structure. This would be the case, for example, when a high angle boundary containing many good nucleation sites surrounds the entire grain. In this instance, although the grain diameter would be representative of the true value, the orientation of the furrows would not necessarily bear a simple relationship to the grain orientation.

In the case of small subgrains, good nucleation sites probably do not exist along all the sub-boundaries, and so nucleation occurs at specific locations only. On growth, one set of furrows can be expected to extend until another is encountered. In this case, no simple relationship can exist between the average subgrain size obtained from optical microscopy and that from transmission electron microscopy.

8.4 VARIATION IN THE GENERAL FEATURES OF THE OXIDE TOPOGRAPHY FOR DIFFERENT CRYSTALLOGRAPHIC PLANES OF SECTION

A preliminary investigation was carried out in which an

attempt was made to correlate the different substructural patterns with the crystallography of the substrate. In this investigation it was found, by repeated repolishing and re-etching, that each of the optical substructures was qualitatively reproducible (Chapter 5), so that each type of apparent substructure seemed to bear some relation to the metal substrate. It was also seen from the scanning electron microscopy that the different optical substructures were associated with definite topographic characteristics (Chapter 7). Further investigations were then carried out to determine in more detail the connection between substrate crystallography and oxide topography. The following investigations were performed and will be discussed in turn:

- (a) a study of transverse sections (Section 5.1, 6.1)
- (b) sectioning of single fibers in different planes (Section 5.2)
- (c) electron diffraction studies of the different substructure types (Section 6.2).

8.4.1 Study of Transverse Sections. During the metallographic observation of transverse sections, it was usually observed that no furrow structure existed on the oxide surface, and that very little contrast could be obtained optically between adjacent subgrains or even fibers (Fig. 15d). From a brief survey of the literature, it was also found that extrusion of aluminum in the temperature range of 400-500°C leads to a duplex $\langle 111 \rangle$, $\langle 100 \rangle$ fiber texture, with the former being more pronounced (90-100%) (73, 74). In a transverse section then, the plane of section is

likely to be a (111) plane. Therefore, the areas without furrows and without an optically visible substructure can probably be associated with {111} lattice planes. (This conclusion is being verified by means of selected area electron diffraction.)

84.2 Sectioning of Single Fibers in Different Planes. Since the $\langle 111 \rangle$ fiber texture is predominant in aluminum extrusions, on taking longitudinal sections, any plane containing the [111] axial direction may be exposed. So it is possible for larger misorientations to exist between adjacent regions than are obtained on transverse sectioning. This is why so much more contrast between fibers is produced on longitudinal sectioning than on transverse sectioning.

On taking various planes of section across a given fiber, a number of different apparent substructures are produced, which are separated by definite angular distances, as seen in Section 5.2. It can therefore be concluded that some correlation must exist between the different substructural patterns observed and the plane of section of the specimen. This topic is considered in more detail below.

84.3 Correlation Between the Type of Substructure Observed Optically and the Crystallography of the Substrate. From electron diffraction studies (Section 6.2) it was found that, when an equiaxed region is observed after polishing and etching, the plane of section is generally in the vicinity of the {310} and {210} planes. Similarly the planes of section in the vicinity of the {110} plane were found to be associated with definitely cross-hatched substructures.

The results obtained by sectioning fibers at different angles with respect to a reference plane can also be used to clarify the relationship between the optically visible substructure and the crystallographic plane of section. Noting that the optical substructure is closely related to the oxide topography, as will be discussed in more detail in Sections 8.5 to 8.8 below, it can be seen (Table II) that the angular distances between the successive patterns correspond generally to the circumferential distances presented on the stereographic plot (Fig. 12). However, the exact orientation of the plane of section at the boundary between two types of substructure is difficult to specify, since the patterns are part of a continuous spectrum.

When the results of the present author on substructures are compared with those of previous workers on recrystallized material, it can be seen from the composite part of the stereogram that excellent agreement is obtained. Considering the work of Bucknell et al., it is seen that for the substrate orientations at which these authors observed a furrow structure on the oxide surface, the scanning electron microscope also showed a definite furrow structure. These areas corresponded to either an equiaxed or a definitely cross-hatched substructure. The regions in which no definite furrow structure was observed by Bucknell corresponded, in the present work, to areas of ⁱⁿ definite cross-hatching, or of no optically visible substructure. Here again, scanning electron metallography showed that no furrows were developed on the oxide surface.

The work of Huber et al. is also in agreement with the present results, although they ascribed the effect to the optical activity of the oxide, and to a related mechanism which, in the view of the present author, is incorrect. Disregarding their interpretation of the effect and looking only at their results, it can be seen that the planes of section for which they observed no rotation of the polarized light are in agreement with those found in the present work on which no furrow structure was seen. Similarly, the substrate orientation of the areas that Huber et al. concluded had optical activity correspond to planes of section possessing well-developed furrows, as revealed by electron microscopy.

From this it can be seen that a loose relationship can be obtained between the type of substructure observed on optical examination, and the plane of section of the polished surface.

8.5 EFFECT OF OXIDE THICKNESS ON APPARENT MICROSTRUCTURES

When plane polarized light is incident on a specimen of anodized aluminum, it was shown in Chapter 3 that a number of different effects could be responsible for producing rotation of the plane of polarization of the reflected light. From the results of the experiments performed in this work, it was concluded that the effect on polarized light was due to the topography of the surface of the oxide. This conclusion was based on the following considerations.

If rotation of the plane of polarization occurred during

the transmission of polarized light through the oxide, then varying the thickness of the oxide would necessarily cause a change in subgrain contrast. This is so since the angle of rotation is the product of the specific rotation and the total thickness of the material. However, subgrain contrast did not change with oxide thickness, as was shown in Fig. 17.

Another point of consideration is that when white polarized light is passed through an optically active material, rotary dispersion is observed, since light of different wavelengths is rotated by different amounts. Such dispersion was not detected. Therefore, the possibility that the rotation of the plane of polarization was due to the optical activity of the oxide was eliminated.

On varying the thickness of the oxide coating, it was also noticed that:

- (a) for very thin coatings, no contrast was produced;
- (b) over a large range of intermediate thicknesses, good contrast was produced;
- (c) after extensive anodizing, the contrast began to disappear.

These results are consistent with the mechanism of polarization by reflection from furrows, as can be seen from the following:

- (i) (a) above can be due to the presence of the amorphous barrier layer, unaccompanied by a well-developed superstructure of furrows;
- (ii) (b) above can be associated with an evenly furrowed surface, as illustrated in the scanning

electron micrographs;

- (iii) (c) can result from the coarsening of the furrow structure which accompanies over-anodizing (48).

8.6 EFFECT OF ANGLE OF TILT ON CONTRAST BETWEEN SUBGRAINS

It was found, (Section 5.5), that contrast between regions increased slightly for small angles of tilt, and that it decreased for angles above 4° . These results are also consistent with a mechanism which involves reflection from the furrow surfaces. According to this model, when a small tilt angle is introduced, the angle of incidence on certain faces of the furrows is increased, thereby increasing the amount of light reflected from these sides. Simultaneously, in neighbouring regions which are near the furrow orientation for extinction, tilting can decrease the amount of light reflected, so that contrast between the regions is increased.

Above about 4° of tilt, the decrease in contrast can be attributed to the following cause. At increasing angles of tilt, only one face of each furrow is active, and the angle of incidence on this face is decreased by the tilt, making polarization by reflection less effective.

8.7 EFFECT OF FURROW DIRECTION ON POLARIZATION BY REFLECTION

It was established above that rotation of the polarized light was not due to the transmission of light through the oxide. It remains to be determined whether or not the effect is due to reflection from the surface of the oxide, or from the metal/oxide interface.

In Section 5.9 it was shown that the deposition of an opaque metal coating over the oxide surface did not significantly alter the effect of the surface on the reflected polarized light. This then establishes that the relevant reflection takes place at the air/oxide interface, and not at the oxide/metal interface. It remains now to examine the details of the effect of furrow direction and slope on the furrow reflection mechanism.

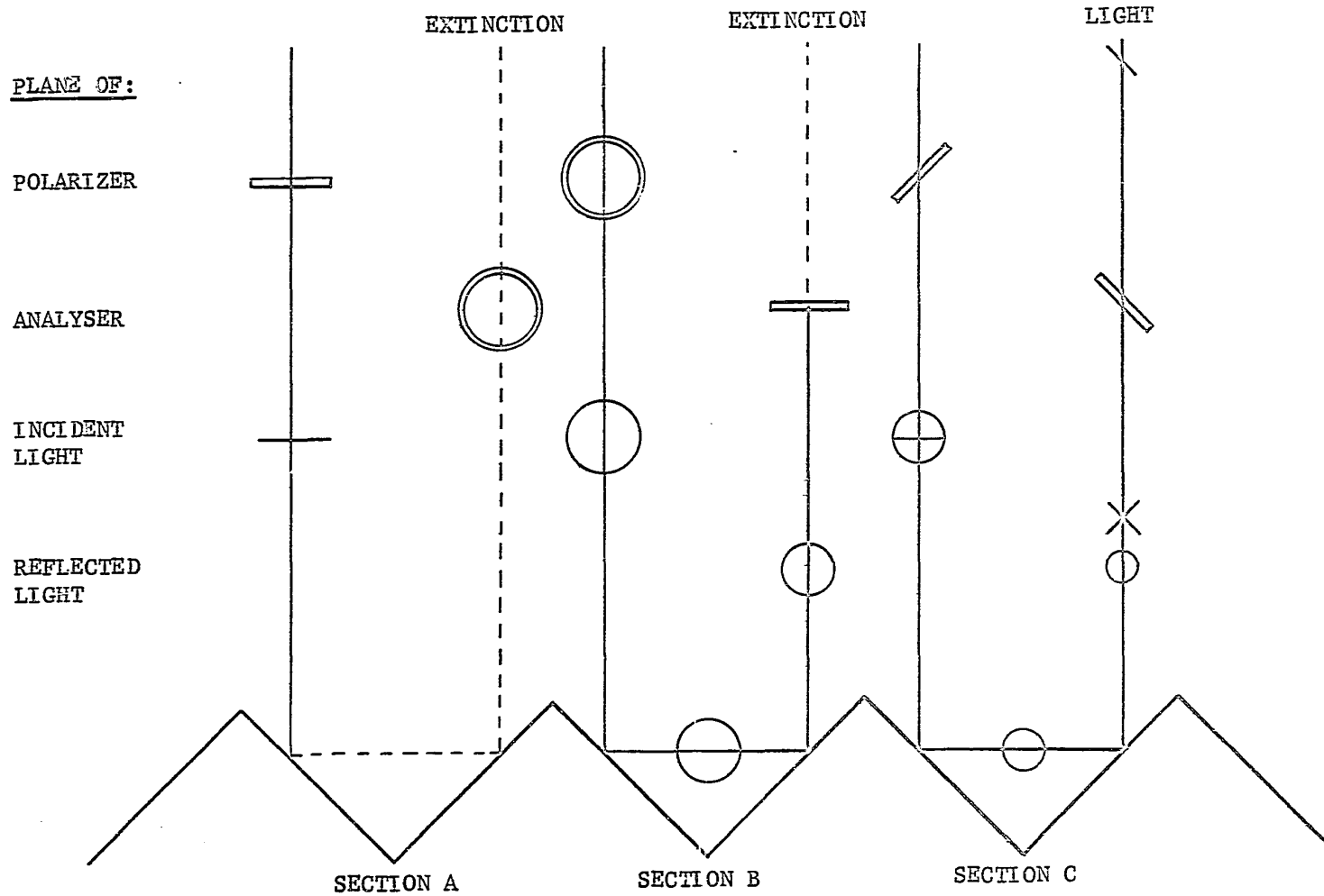
The angle between the furrow direction and the plane of polarization of incident light determines the brightness of a given grain or subgrain, as can be seen on consideration of Fig. 28. In section A, the plane of the polarizer is in the plane of the page, while the idealized grooves are perpendicular to the plane of the page. In this case, as can be seen from the theory of reflection, very little light is reflected from the surface of first incidence, since the plane of vibration is perpendicular to the plane of incidence. This results in extinction for the particular grain or subgrain.

In section B, the plane of vibration is parallel to the plane of incidence, and so a large proportion of the incident light

FIGURE 28

Reflection of the polarized light from an idealized furrow structure, for different orientations of the plane of the polarizer, with respect to the furrow direction.

OBSERVED:



-  : plane of polarizer or analyser perpendicular to furrow direction.
-  : plane of polarizer or analyser parallel to furrow direction.
-  : plane of polarized light perpendicular to furrow direction.

is reflected from each surface. The percentage of light reflected depends only on the angle of incidence, and upon the reflectance of the surface at that particular angle. The latter was seen previously to depend on the refractive index of the material. After the light in this case is reflected from the furrowed surface, its plane of vibration is perpendicular to the plane of the paper. This light is then absorbed by the analyser, resulting in extinction.

In section C, where the plane of the polarizer is at an angle other than 0° or 90° to the direction of the furrows, the incident polarized light can be resolved into components perpendicular and parallel to the direction of the furrows. At the first face, the component parallel to the furrow direction is reflected much more strongly than the other component, and it is again reflected more strongly at the second face, continuing to the analyser. If components of this vibration are now taken parallel and perpendicular to the plane of the analyser, it will be seen that only the component parallel to the analyser is transmitted. Thus this particular grain or subgrain appears bright compared to the appearance of areas with furrows perpendicular or parallel to the incident plane of polarization (sections A and B). From geometry it can be seen that the position of maximum brightness for a given grain or subgrain is at a furrow direction of 45° to the plane of polarization of the incident light.

Considering for the moment that the furrow direction is the sole factor affecting the contrast between adjacent grains or subgrains,

the values of "misorientation" given in Section 5.3 can be taken to represent the differences in furrow orientation between subgrains. This can be made clearer by referring to Fig. 29. In this diagram, AA represents the plane of the analyser, and LL and SS represent the major and minor axes, respectively, of the elliptically polarized light reflected from the surface of grain A. Similarly, NN and UU represent the light from grain B.

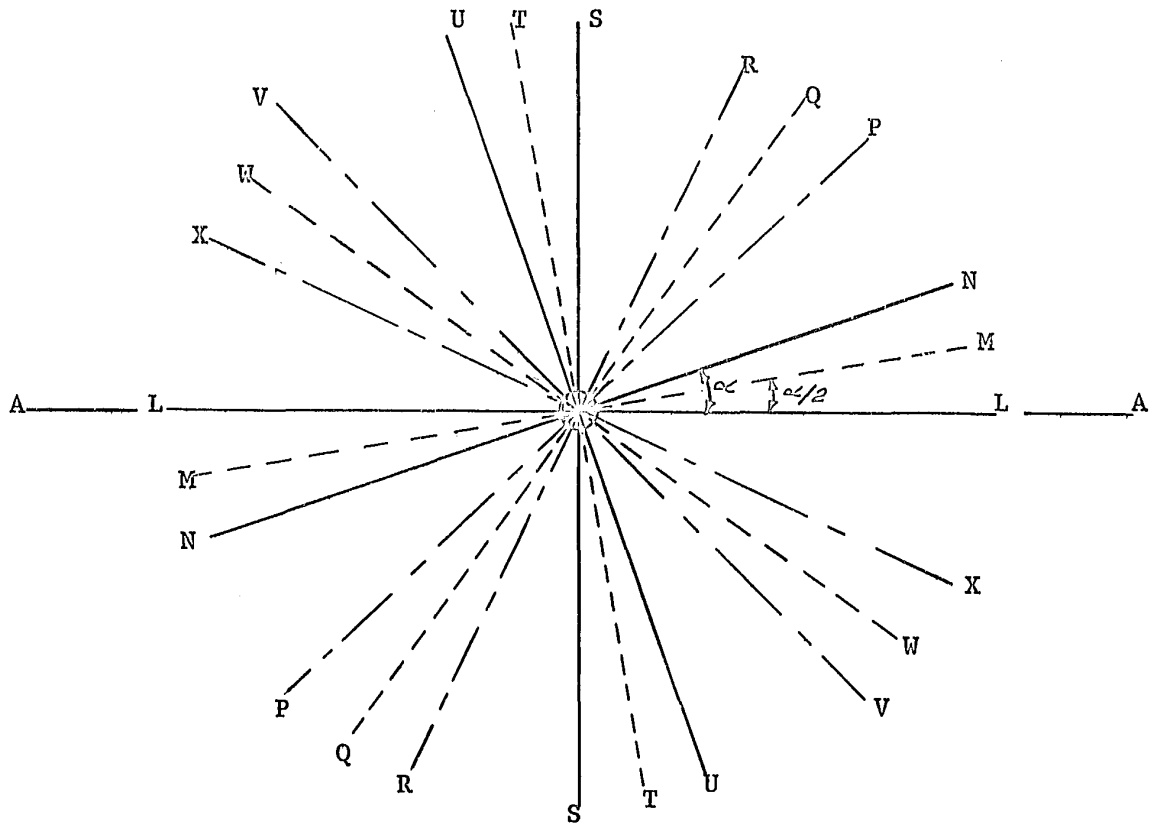
Under these conditions, the LL component of the light reflected from grain A will be totally transmitted through the analyser, while the SS component will be totally absorbed. The NN component of the light reflected from grain B will also be almost totally transmitted, though not completely so. In addition to this, part of the component along the minor axis will also be transmitted through the analyser.

In this condition, both grains A and B appear very bright, though A is actually brighter than B. Since the response of the human eye to light intensities is markedly non-linear, and less sensitive in the higher intensity ranges, both grains appear equally bright. These orientations of A and B thus produce the "white field" seen in the microscope, the center of which is represented by MM. Also, for this position of grain A, the furrows must be at 45° to AA, i.e., either parallel to PP or parallel to VV.

On rotating grains A and B through 45° from their original positions, so that the furrows of grain A are now either parallel or perpendicular to AA, (i.e. PP is in the plane of the analyser), the

FIGURE 29

Schematic representation of the axis of polarization of light reflected from two subgrains, and the angular location of the various fields of view observed.



- A A: plane of analyser
 L L: major axis of elliptically polarized light reflected from grain A
 S S: minor axis of elliptically polarized light reflected from grain A
 N N: major axis of elliptically polarized light reflected from grain B
 U U: minor axis of elliptically polarized light reflected from grain B
 M M; T T: white field
 P P, V V: structure A
 Q Q, W W: dark field
 R R, X X: structure B
 $\angle \text{LON} = \alpha = \text{misorientation}$
 $\angle \text{MOQ} = 45^\circ$
 $\angle \text{MOT} = 90^\circ$
 $\angle \text{POX} = 90 + \alpha$
 $\angle \text{LOM} = \alpha/2 = \angle \text{POQ} = \angle \text{QOR}$
 $\angle \text{SOT} = \angle \text{TOU}$
 $\angle \text{VOW} = \angle \text{VOX}$

light from grain A transmitted through the analyser is at a minimum, causing it to appear very dark. While in this position, grain B still transmits a certain amount of light as its furrows are not quite perpendicular or parallel to AA. This produces a high degree of contrast between the subgrains, and is called structure A. On further rotation through the angle POQ, both grains A and B transmit the same very small amount of light, so that both appear very dark. This position is the so-called "dark field" seen under the microscope. On further rotation through the small angle QOR, grain B grows darker and grain A lighter until, at maximum contrast, the furrows of grain B are aligned parallel or perpendicular to AA, the plane of the analyser. Here grain B is very dark, and grain A is light in comparison. This is termed "structure B".

From the above it can be seen that the structure A to structure B angular distance is the angle POR, and that this is the apparent misorientation between the subgrains. However, it would be more accurate to say that the angle POR is the angle between the furrow directions in the two grains and, as has been discussed above, since these furrow directions are not epitaxially related to the substrate crystallography, the "misorientation" is not a true crystallographic misorientation, but only an apparent one. It can also be seen that the angular distance from black field to white field is 45° , and that the cycle: white field/structure A/dark field/structure B/white field is repeated every 90° .

8.8 EFFECT OF FURROW SLOPE ON POLARIZATION BY REFLECTION

It was seen above that the furrow orientation in a given area affects the apparent brightness of the area when it is viewed through crossed polarizers. The inclination of the furrow faces to the horizontal also affects the brightness of the area, as can be seen from the simplified model which is illustrated in Fig. 30. In this case, the incident plane polarized light has a mean amplitude E at an azimuth angle ψ_E . This incident light can be resolved into two components E_p and E_s^* . The amplitude of E_s is $E \cos \psi_E$, and that of E_p is $E \sin \psi_E$.

From equation 4 in the theory, it can be seen that

$$\frac{R_s}{E_s} = - \frac{\sin (\theta - \theta')}{\sin (\theta + \theta')}$$

and

$$\frac{R_p}{E_p} = \frac{\tan (\theta - \theta')}{\tan (\theta + \theta')}$$

Thus the light amplitudes at point Q of the figure can be expressed in terms of E_s and E_p , the angle of incidence θ , and the angle θ' , which is defined as follows:

$$\sin \theta' = (\sin \theta)/n$$

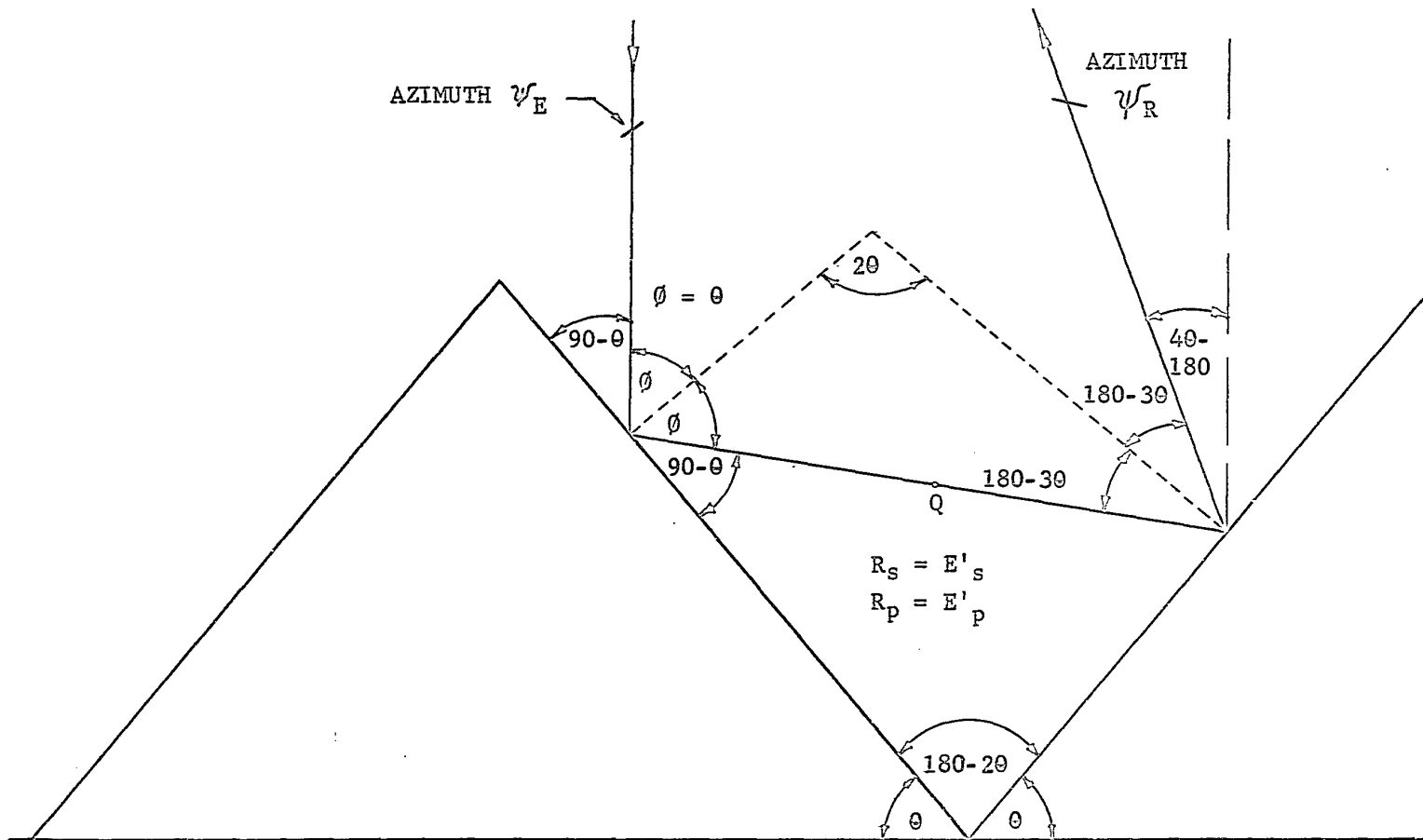
Here n , the index of refraction, is constant for a given material, and E_s and E_p are also constant for a given furrow orientation with respect to the plane of the polarizer. Therefore both R_s and R_p are functions of θ alone.

Now R_s and R_p can be considered as the light components incident on surface B, so they can be denoted as E'_s and E'_p ,

* All the following notation is as described in Chapter Three.

FIGURE 30

The effect of furrow slope on the intensity
of the reflected polarized light.



Note: The angle $4\theta - 180^\circ$ is usually very small, but has been exaggerated here for clarity.

respectively, with respect to this surface. Again, by Fresnel's law, the reflected light R'_s and R'_p can be found. In this case R'_s and R'_p are functions of E'_s and E'_p and the new angle of incidence θ_1 . By the geometry of the configuration, θ_1 can be expressed in terms of θ , the original angle of incidence, and the angle of inclination of the furrow face. Now for vertically incident light, the angle of incidence θ is equal to θ , the angle of inclination of the furrow face, so that R'_s and R'_p , the reflected light amplitudes, can be expressed as functions of the furrow slope alone, all other parameters remaining constant.

However, the intensity of the light reflected from a given area is not actually the intensity that is observed through the eyepiece of the microscope, since only the component parallel to the analyser is transmitted. The magnitude of this component is dependent on ψ_R , which is $\tan^{-1} \frac{R'_p}{R'_s}$, so that the intensity of the light passing through the analyser is still a function of θ alone (once n and ψ_E are fixed).

For the simplified furrow structure shown in Fig. 30, the values of R'_s and R'_p have been found to be the following:

$$R'_s = E \cos \psi_E \left[\frac{\sqrt{n^2 - \sin^2 \theta} - \cos \theta}{\sqrt{n^2 - \sin^2 \theta} + \cos \theta} \right] \left[\frac{\sqrt{n^2 - \sin^2 3\theta} + \cos 3\theta}{\sqrt{n^2 - \sin^2 3\theta} - \cos 3\theta} \right]$$

$$R'_p = E \sin \psi_E \left[\frac{\tan \theta \sqrt{n^2 - \sin^2 \theta} - \sin \theta}{\sqrt{n^2 - \sin^2 \theta} + \tan \theta \sin \theta} \right] \left[\frac{\sqrt{n^2 - \sin^2 \theta} - \tan \theta \sin \theta}{\tan \theta \sqrt{n^2 - \sin^2 \theta} + \sin \theta} \right]$$

$$\times \left[\frac{\sin 3\theta + \sqrt{n^2 - \sin^2 3\theta} \tan 3\theta}{\sqrt{n^2 - \sin^2 3\theta} - \tan 3\theta \sin 3\theta} \right] \left[\frac{\sqrt{n^2 - \sin^3 3\theta} + \tan 3\theta}{\tan 3\theta \sqrt{n^2 - \sin^3 3\theta} - \sin 3\theta} \right]$$

A more realistic model of the actual furrow structure is the one shown in Fig. 31, based on sharp peaks and semicircular valleys. In this case, two or more reflections can occur, each being governed by the value of θ , or of α' , where

$$\alpha' = \sin^{-1} \left[\sin \theta - \left(\frac{PW - PU}{OB} \right) \right]$$

(Each of these symbols is defined on the diagram.)

In the latter case, the reflected light is not only a function of θ , but also of the elevation at which first incidence is made, and of the radius of the valley. The latter quantities are again dependent solely upon the geometry of the furrow structure, since for vertically incident light, ϕ is equal to θ .

From these considerations, it can be seen that the degree of rotation of the reflected polarized light is dependent not only on the furrow orientation, but also on the furrow slope. Thus the contrast which is apparent between neighbouring regions can be attributed to different furrow densities and configurations in adjacent areas. These different furrow configurations are not, however, uniquely related to the crystallography of the underlying metal.

FIGURE 31

The effect of furrow geometry on the intensity of the reflected polarized light.

CHAPTER NINE

CONCLUSIONS

The following are the conclusions of this study.

1. The type of optical substructure observed after electrolytic polishing and etching is loosely dependent on the plane of section of the specimen. An equiaxed substructure is observed when the plane of section is in the vicinity of the (120), (130) planes; the definitely cross-hatched pattern when the plane is in the vicinity of the (110) or (230); while the indefinitely cross-hatched pattern is seen when sections expose the (150) and (100). No substructure is seen in the vicinity of the (111) plane.
2. When subgrains can be detected optically, the measured subgrain sizes are misleading, and are usually larger than the values obtained by transmission electron metallography. This is particularly true for small subgrains (1 - 10 microns diameter).
3. The values of subgrain misorientation determined by the use of polarized light and stage rotation are anywhere up to an order of magnitude larger than the values obtained by electron diffraction. The optically-determined misorientations are thus judged to be unreliable.
4. The different optical substructures are associated with certain topographic features of the outer oxide layer. The best subgrain contrast is produced when parallel furrows are formed on the oxide surface, in agreement with previous work on coarse-grained recrystallized aluminum.

5. The outer oxide layer nucleates and grows on an intermediate layer of amorphous oxide. Thus, the outer oxide layer is not epitaxially related to the metal substrate, and the structure of the outer layer is only loosely related to the crystallography of the metal.
6. The response to polarized light is mainly due to reflection from the striated surface of the oxide, and very little, if at all, to transmission through the oxide layer, or to reflection at the metal/oxide interface.
7. When the striations or furrows are either perpendicular or parallel to the plane of polarization of the incident light, extinction occurs.
8. The angle of rotation of the plane of polarization is dependent not only on the orientation of the furrows with respect to the plane of polarization, but also on the slope or density of the furrows.
9. From the above statements, it may be seen that the electrolytic polishing and etching of aluminum can, under favourable conditions, establish the presence of a substructure. However, for subgrain sizes less than about 10 to 15 microns, the sizes and misorientations observed optically are neither uniquely nor simply related to the true structure of the metal substrate.

APPENDIX

STRAIN ANNEALING OF EXPERIMENTAL BILLETS

During extrusion, a polycrystalline billet suffers a large reduction in cross-section, and simultaneously undergoes a corresponding amount of elongation. This means that a so-called "fibrous" microstructure results after extrusion, as long as recrystallization does not occur. In previous work at McGill (1), it was found that the diameter of each of these fibers is related to the original grain size by the square ²root of the extrusion ratio. To carry out the present investigation, it was found necessary to use a fiber diameter of 1 - 3 mm. in extrusions, and so a grain size of 3 - 10 mm. was required in the starting material.* To obtain this grain size, strain annealing techniques were employed.

A review of the principles of strain annealing and of the various factors influencing this process has been published by Gilman (71). In the present work, coarse-grained extrusion billets were prepared according to the following procedure.

1. The as-received material was cut into 4 inch lengths, faced, and identified. It was then pre-annealed in an air furnace at 640° C for three hours. The pre-anneal was employed to ensure that the specimen was strain free and that the starting grain size was reasonably uniform.
2. After cooling, the billets were strained in compression by the amounts listed in Table A-1. Compression

* Using an extrusion ratio of 10:1.

was performed using the vertical extrusion press, and to ensure uniform straining, grease was liberally applied to the top and bottom faces of the billets. The length of each billet was measured before compression using a 10 inch inside-outside vernier caliper. The reduction in length was then calculated for the required percent of strain and this value was set on the calipers. These were placed next to the billet to provide a visual indication of the required ram travel.

3. After deformation, the billets were cleaned with varsol, and the final lengths were again measured to the nearest thousandth of an inch. From this, the actual strain percentages were calculated.
4. The billets were then replaced in the air furnace and annealed at 640°C for 48 hours.

To check the grain sizes, strain-annealed billets were sectioned longitudinally, polished, and etched in a modified Tucker's etch consisting of:

H ₂ O (Distilled)	30% by volume
HCl	30% by volume
HNO ₃	30% by volume
HF (48%)	10% by volume.

From Table A-1, it can be seen that the largest grain size was obtained under the following conditions:

Preanneal at 640°C for 3 hours.

Strain in compression 3.8 - 4.0%.

Final anneal at 640°C for 48 hours.

TABLE A-1

STRAIN ANNEALING TEST RESULTS

<u>% Strain</u>	<u>Billet No.</u>	<u>Test No.</u>	<u>Remarks</u>
1.00	1	-	Very fine grain size.
2.10	2	-	Very mixed grain size.
3.00	3	-	Few large grains (5 x 40 mm), mostly very small (approx. 1 mm).
3.57	7	-	Mixed very large (10 x 40 mm) and medium sized (5 x 10 mm) grains, non-uniformly distributed.
3.80*	42	-	Small to medium sized grains, fairly evenly distributed.
3.85	9	-	Very large grain (15 x 30 mm) at center, rest large sized, elongated grains.
3.87	15	7	-
3.90	40	4	-
3.95	8	2	-
3.95	13	11	-
3.97	11	12	-
3.97	14	8	-
4.00*	43	-	Fairly large equiaxed grains, uniformly distributed.
4.08	12	10	-
4.09	16	5	-
4.14	5	1	Mostly large (5 x 20 mm) and few small (2 mm) grains.
4.31	10	-	Mostly fine grains, with large elongated grains at the skin.
5.51	6	-	Very fine grain size (approx. 3 mm).

Note: The above billets were pre-annealed at 640°C for 3 hours, strained as shown, and final annealed at 640°C for 48 hours.

* These billets were treated as above, but the final annealing conditions were 640°C for 19 hours.

BIBLIOGRAPHY

1. W. A. WONG, H. J. McQUEEN, J. J. JONAS
J. of the Inst. of Metals, to be published, 1967 .
2. H. J. McQUEEN, W. A. WONG, J. J. JONAS
Can. J. Phys., to be published Feb. 1967.
3. G. KORTUM AND J. BOCKRIS
"Electrochemistry", Vol. 2, Elsevier Publishing Co.,
Amsterdam.
4. D. A. MacINNES
"The Principles of Electrochemistry", Dover, New York, 1961.
5. W. J. McG. TEGART
"The Electrolytic and Chemical Polishing of Metals",
Pergamon Press, 1959.
6. P. A. JACQUET
Metal Finishing, 47 (5), 48, 1949.
7. W. C. ELMORE
J. of Applied Physics, 10, 727, 1939.
8. *ibid.* 11, 797, 1940.
9. M. HALFAWY
Experimentia, 7, 175, 1951.
10. J. EDWARDS
J. Electrochemical Soc., 100, 189c, 1953.
11. U. R. EVANS, D. WHITWHAM
J. Electrodepositors' Tech. Soc., 22, 24, 1947.
12. P. A. JACQUET
Met. Reviews, 1, 170, 1956.
13. D. LaFROGUE-KANTZER
Comptes Rend., 233, 547, 1951.
14. U. R. EVANS
"Discussions on Electrolytic Polishing", 3rd Internat.
Conf. on Electrodeposition, London, 1947.

15. E. DARMOIS, D. AMINE
Comptes Rend., 237, 501, 1953.
16. P. BROUILLET
Metaux Corrosion Ind., 30, 141, 1955.
17. *ibid.* 30, 192, 1955.
18. *ibid.* 30, 243, 1955.
19. H. RAETHER
Comptes Rend., 227, 1247, 1948.
20. *ibid.*
Metaux et Corrosion, 25, 1, 1950.
21. G. L. KEHL
"The Principles of Metallographic Laboratory Practice",
McGraw-Hill, p. 409, 1949.
22. H. EVANS
"Conference on the Microscopy of Metals", London, p. 24, 1953.
23. P. A. JACQUET
Met. Reviews, 1, 212, 1956.
24. P. MICHEL
Sheet Metal Ind., 26, 2175, 1949.
25. P. A. JACQUET
C. R. Acad. Sci., Paris, 227, 556, 1948.
26. L. YOUNG
"Anodic Oxide Films", Academic Press, New York, 1961.
27. U. R. EVANS
"The Corrosion and Oxidation of Metals", Arnold, London, 1960.
28. J. E. LEWIS, R. C. PLUMB
J. Electrochemical Soc., 105, 496, 1958.
29. G. AMSEL, D. SAMUEL
J. Phys. Chem. Solids, 23, 1707, 1962.

30. Th. RUMMEL
Z. Phys., 99, 518, 1936.
31. J. A. DAVIES, J. P. S. PRINGLE, R. L. GRAHAM, F. BROWN
J. Electrochemical Soc., 109, 999, 1962.
32. J. A. DAVIES, B. DOMELJ
ibid. 110, 849, 1963.
33. J. P. S. PRINGLE, J. A. DAVIES
Paper presented at the Pittsburgh Meeting of the
Electrochemical Soc., April 1963, Abstract No. 167.
34. J. A. DAVIES, B. DOMELJ, J. P. S. PRINGLE, F. BROWN
J. Electrochemical Soc., 112, 675, 1965.
35. F. KELLER, M. S. HUNTER, D. L. ROBINSON
J. Electrochemical Soc., 100, 411, 1953.
36. H. A. RAETHER
Metaux et Corrosion, 25, 1, 1950.
37. A. F. BROWN
Nature, 163, 961, 1949.
38. G. L. BUCKNELL, G. A. GEACH
Nature, 164, 231, 1949.
39. N. C. WELSH
J. Inst. of Metals, 85, 129, 1956-1957.
40. G. L. BUCKNELL, G. A. GEACH, N. C. WELSH
Research, 5, 289, 1952.
41. P. BUSSY
Rev. Met., 52, 116, 1955.
42. A. HONE, E. C. PEARSON
Metal Progress, 53, 363, 1948.
43. ibid. 58, 713, 1950.
44. E. C. PEARSON, G. MARCHAND, R. H. HAY
Trans. Canadian Inst. Mining & Met., 55, 348, 1952.

45. M. PAGANELLI
Aluminio, 27, 3, 1958.
46. L. BEAUJARD, P. LACOMBE
Journées des États de Surface, p. 44, 1945.
47. E. C. W. PERRYMAN
Acta Metallurgica, 2, 26, 1954.
48. K. HUBER, A. GANGLER
Experimentia, 3, 277, 1947.
49. F. A. JENKINS, H. E. WHITE
"Fundamentals of Optics", McGraw-Hill, New York, 1957.
50. R. W. WOOD
"Physical Optics", Macmillan, New York, 1919.
51. P. DRUDE
"The Theory of Optics", Longmans, Green & Co., New York, 1907.
52. J. K. ROBERTSON
"Introduction to Optics", D. Van Nostrand, 1957.
53. W. A. WOOSTER
"A Textbook on Crystal Physics", 1938.
54. O. WIENNER
Ann. Physik, 40, 203, 1890.
55. JAMIN
ibid. 19, 296, 1847.
56. R. W. DAYTON
Trans. Amer. Inst. of Mining & Met. Eng., 117, 119, 1935.
57. B. W. MOTT, H. R. HAINES
Research, 4, 24, 1951.
58. N. C. WELSH
ibid. 8, 528, 1955.

59. H. WILSDORF, D. KUHLMANN-WILSDORF
"Report on the Conference on Defects in Crystalline Solids",
held at the H. H. Wells Phys. Lab., Univ. of Bristol,
July, 1954, p. 175.
60. H. BERGHEZAN
Metaux Corr. Ind., 30 (359-360), 269, 1955.
61. L. J. BARKER
Trans. Amer. Soc. for Metals, 42, 347, 1950.
62. D. H. WOODARD, E. L. BRONSON
Nature, 168, 742, 1951.
63. E. C. W. PERRYMAN, J. M. LACK
ibid. 167, 479, 1591.
64. M. BAEYERTZ
Trans. Amer. Inst. Min. Met. Eng., 117, 151, 1935.
65. W. A. WONG
M. Eng. Thesis, Dept. of Metallurgical Eng., McGill
University, 1965.
66. O. JONES
Philosophical Mag., 48, 207, 1924.
67. J. E. HILLIARD
Metal Progress, 85 (5), 99, 1964.
68. K. C. A. SMITH, C. W. OATELY
Brit. J. of Appl. Phys., 6, 391, 1955.
69. J. S. KOHLER
Phys. Rev., 75, 106, 1949.
70. ibid.
Amer. J. Phys. 10, 275, 1942.
71. R. LANDAUER
Phys. Rev., 82, 520, 1951.

72. J. HERENGUEL, P. LeLONG
C. R. Acad. Sci., Paris, 232, 2218, 1951.
73. C. S. BARRETT
"Structure of Metals", McGraw-Hill, New York, 1952.
74. I. L. DILLAMORE
Met. Reviews, 10 (39), 271, 1965.
75. Y. C. LIU
Trans. Amer. Inst. Min. Met. Eng., 230, 1513, 1964.
76. J. J. GILMAN
"The Art and Science of Growing Crystals", John Wiley and
Sons, 1963.